Synergistic melanoma cell death mediated by inhibition of both MCL1 and BCL2 in high-risk tumors driven by NF1/PTEN loss

Synergistic melanoma cell death mediated by inhibition of both MCL1 and BCL2 in high-risk tumors driven by NF1/PTEN loss

Shuning He[1,*], Mark W. Zimmerman[1], Hillary M. Layden[1], Alla Berezovskaya[1], Julia Etchin[1], Megan W. Martel[1], Grace Thurston[1], Chang-Bin Jing[1], Ellen van Rooijen[2], Charles K. Kaufman[2], Scott J. Rodig[3], Leonard I. Zon[2], E. Elizabeth Patton[4], Marc R. Mansour[1,5,*], and A. Thomas Look[1,*]

[1]Department of Pediatric Oncology, Dana-Farber Cancer Institute, Harvard Medical School, Boston MA, 02115, USA.

[2]Stem Cell Program and Division of Hematology/Oncology, Children's Hospital Boston, Howard Hughes Medical Institute, Boston, MA, 02115, USA.

[3]Department of Pathology, Brigham and Women's Hospital, Boston, MA, 02115, USA.

[4]MRC Human Genetics Unit, MRC Institute of Genetics and Molecular Medicine, University of Edinburgh, Crewe Road South, Edinburgh, EH4 2XR, UK.

[5]Department of Hematology, UCL Cancer Institute, University College London, WC1E 6BT, UK.

*To whom correspondence should be addressed: shuning_he@dfci.harvard.edu (S.H.), m.mansour@ucl.ac.uk (M.R.M), Thomas_Look@dfci.harvard.edu (A.T.L.)

Competing interests: The authors have declared that no conflict of interest exists.

Abstract

Melanomas driven by loss of the NF1 tumor suppressor have a high risk of treatment failure and effective therapies have not been developed. Here we show that loss-of-function mutations of *nf1* and *pten* result in aggressive melanomas in zebrafish, representing the first animal model of NF1-mutant melanomas harboring PTEN loss. MEK or PI3K inhibitors show little activity when given alone due to cross-talk between the pathways, and high toxicity when given together. The mTOR inhibitors, sirolimus, everolimus and temsirolimus, were the most active single agents tested, potently induced tumor-suppressive autophagy, but not apoptosis. Because addition of the BCL2 inhibitor venetoclax resulted in compensatory upregulation of MCL1, we established a three-drug combination composed of sirolimus, venetoclax and the MCL1 inhibitor S63845. This well-tolerated drug combination potently and synergistically induces apoptosis in both zebrafish and human NF1/PTEN-deficient melanoma cells, providing preclinical evidence justifying an early-stage clinical trial in patients with NF1/PTEN-deficient melanoma.

Introduction

Cutaneous melanoma accounts for the vast majority of skin cancer-related deaths. More than 100,000 newly diagnosed cases of melanoma are projected in the United States for 2020 together with ~6,800 melanoma-related deaths[1]. The Cancer Genome Atlas (TCGA) classified cutaneous melanomas into four molecular subtypes: *BRAF*-mutant (47.5%), *RAS*-mutant (29%), *NF1*-mutant (9%), and triple-wild-type (14.5%)[2]. The *NF1*-mutant category refers to cases lacking either *BRAF* or *RAS* mutations, whereas *NF1* mutations can also arise as a mechanism of resistance to RAF/MEK-targeted therapies in *BRAF*-mutated melanoma[3,4]. Thus, *NF1* mutations have been reported in 13-17% of cutaneous melanomas overall[2,5,6].

The *NF1* gene encodes neurofibromin, a 2818-amino-acid protein whose GTPase-activating protein-related domain negatively regulates RAS signaling by catalyzing the hydrolysis of RAS-GTP into RAS-GDP. Thus, one consequence of *NF1*-loss is the aberrant activation of RAS signaling[7]. In primary melanoma patient biopsies, *NF1* mutations were not correlated with hot-spot *BRAF* mutations, a finding consistent with a redundant role for these two types of mutations in activating RAS-MAPK signaling.

Recent efforts to develop improved targeted therapies for melanoma have mainly focused on the *BRAF*-mutant subtype, leaving a paucity of treatment options for patients with *NF1*-mutant melanomas. It is unlikely that the FDA-approved BRAF-mutant-specific inhibitors will be beneficial against *BRAF*-wild-type, *NF1*-mutant melanomas. Moreover, analysis of multiple clinical trials indicate that the *NF1*-mutant subtype has the worst outcome among all metastatic melanomas[8]. Clearly, a better understanding of the molecular pathogenesis of *NF1*-mutant melanomas is needed to improve the design and hence the outcome of treatments for this subtype of melanoma.

A major impediment to the development of targeted therapies for patients with *NF1*-mutant melanomas has been the lack of suitable animal models. For example, both the *BRAF*-mutant and

RAS-mutant subtypes of melanoma have been successfully modeled in mice[9] and zebrafish[10] by combining the melanoma-associated mutations in these genes with mutation or loss of *p53* or *Cdkn2a*, which are both typically inactivated in human melanoma[2,11]. However, *Nf1*-loss was not sufficient to induce melanoma tumorigenesis in mice[3,12] or zebrafish[13], either alone or in combination with *p53*-loss. As the NF1-mutant melanomas often harbor a high mutation load[14,15], we reasoned that genetic or epigenetic alterations affecting genes other than *p53* and *Cdkn2a* are likely required in combination with *NF1*-loss to initiate melanoma transformation *in vivo*. Because a significant subset of human *NF1*-mutant melanomas harbor genetic alterations leading to activation of the PI3K-AKT-mTOR pathway[2,6], we hypothesized that targeting this pathway through inactivation of *ptena/ptenb* would drive melanomagenesis in *nf1/p53*-mutant zebrafish.

Results

Loss-of-function mutations of *nf1* and *pten* cooperate to drive melanomagenesis in *p53*-deficient zebrafish.

We previously reported the development of *nf1a*$^{+/-}$;*nf1b*$^{-/-}$ zebrafish lines with loss of three of the four functional alleles of *nf1*[13]. These animals develop spontaneous malignant peripheral nerve sheath tumors (MPNSTs) with low penetrance, but not melanomas, beginning at the age of 1.5 years, indicating that *nf1*-loss alone is not sufficient to drive melanomagenesis (Supplementary Figure S1). When we bred the *nf1a*$^{+/-}$;*nf1b*$^{-/-}$ line into a *p53*-deficient (*p53*$^{M214K/M214K}$) background, the compound mutant fish developed MPNSTs or high-grade gliomas[13]. Although rare spontaneous melanomas were also detected, they had a very low penetrance (<2%) over the course of 40 weeks (Supplementary Figure S1). Because human *NF1*-mutant melanomas often harbor gain-of-function alterations in the PI3K signaling pathway, including mutational inactivation of PTEN or overexpression of AKT3[2,6], we introduced *pten* loss-of-function mutations into *nf1a*$^{+/-}$;*nf1b*$^{-/-}$;*p53*$^{M214K/M214K}$ zebrafish by crossing with a previously established *ptena*$^{+/-}$;*ptenb*$^{-/-}$ line[16,17]. We then incrossed *nf1a*$^{+/-}$;*nf1b*$^{+/-}$;*ptena*$^{+/-}$;*ptenb*$^{+/-}$;*p53*$^{+/M214K}$ fish and monitored the offspring for spontaneous tumor development every 2 weeks starting at 5 weeks of age. Very aggressive melanotic tumors began to appear in these fish at 7 weeks of age, with a penetrance of 80% by 20 weeks (Figures 1a-e). Histopathologic study of the melanotic tumors revealed a dense, cellular neoplasm in which a subset of the neoplastic cells produced pigment, with an overall histology pathognomonic of malignant melanoma (Figures 1b-d). Thus, activation of the PI3K pathway appears to be a critical requirement for melanomas to develop, in this case in concert with loss of *NF1* and *p53*.

Melanomas arising in the *nf1/pten/p53*-mutant background were highly invasive into underlying musculature (Figures 1b-d), and developed much earlier than melanomas in either the

Tg(mitf:BRAF^{V600E});p53$^{M214K/M214K}$ or *Tg(mitf:NRAS^{Q61K});p53$^{M214K/M214K}$* zebrafish[18-21]. MPNSTs and glioblastomas appear in the *nf1/p53* background after 30 weeks of age, while melanomas develop starting at 5 weeks of age in the *nf1/pten/p53* background and grow so rapidly that fish usually need to be sacrificed for humane reasons before 30 weeks of age, so melanomas are the only tumor-type observed in the *nf1/pten/p53* background. Importantly, these spontaneous melanomas arose exclusively in fish that were homozygous null for both *nf1b* and *ptenb,* heterozygous for *nf1a* and *ptena* mutant alleles, and either heterozygous or homozygous for *p53^{M214K}* (Figures 1 and S2). DNA PCR from melanoma tumors and adjacent normal tissue showed that the wild-type allele of *nf1a* and *ptena* is retained by the tumor cells (Supplementary Figure S3). The *nf1a$^{+/-}$;nf1b$^{-/-}$;ptena$^{+/-}$;ptenb$^{-/-}$;p53$^{M214K/M214K}$* tumors (designated "*nf1/pten*-mutant melanomas") developed at random sites across the surface of the fish (Figure 1a). The pigmented melanoma cells were highly invasive, infiltrating skeletal muscle adjacent to every tumor examined for histology (Figures 1b-d). Hence, retention of only one allele of both *nf1* and *pten* in a p53-mutant background drives the development of highly invasive malignant melanoma in our zebrafish model.

The *nf1/pten*-mutant melanomas lack *braf/nras* hot-spot mutations.

Since 80% of human cutaneous melanomas harbor activating hot-spot mutations in either *BRAF* or *NRAS* (e.g., *BRAFV600, NRASG12* or *NRASQ61)*[2], we examined the *nf1/pten*-mutant zebrafish melanomas for spontaneous mutations at equivalent sites in the zebrafish orthologues (Supplementary Figure S4). Sequencing of eight tumors revealed only wild-type alleles of these two genes in each tumor (Supplementary Figure S5). Hence, similar to the *NF1*-mutant class of human cutaneous melanomas[2], the loss of *nf1* is sufficient to provide RAS pathway activation, and zebrafish melanomas in this background do not contain *braf/nras* hot-spot mutations.

nf1/pten-mutant melanomas exhibit aberrant activation of the RAS and PI3K pathways and are highly proliferative.

Since NF1 and PTEN are well-established negative regulators of RAS and PI3K signaling[7,22], respectively, we postulated that the *nf1/pten*-mutant melanomas would exhibit activation of effector pathways downstream of *RAS* and *PI3K*. Indeed, we detected high levels of phosphorylated ERK (pERK), phosphorylated AKT (pAKT) and phosphorylated S6 ribosomal protein (pS6, an mTOR downstream effector) by immunohistochemistry (IHC) in the *nf1/pten*-mutant melanomas (Figure 1f), indicating hyperactivation of both RAS and PI3K pathways. Because these pathways drive proliferation, we next analyzed the proliferative capacity of *nf1/pten*-mutant melanomas, observing high levels of expression of proliferating cell nuclear antigen (PCNA) in 45% of tumor cell nuclei but not the adjacent normal tissue (Figure 1f), indicating a high tumor proliferative rate. Apoptotic cells were not observed in these melanomas, as indicated by the lack of detectable cleaved caspase-3 (Figure 1f). Hence, combined activation of the RAS and PI3K pathways, a high proliferative rate and the lack of apoptosis likely account for the rapid onset and high growth rate of *nf1/pten*-mutant melanomas.

nf1/pten-mutant melanomas can be serially transplanted into immunodeficient recipients.

To assess the transplantation potential of our melanoma model, we isolated *nf1/pten*-mutant melanoma cells and transplanted them intraperitoneally into the optically clear immunodeficient *rag2*^{E450fs}*(casper)* zebrafish[23] (designated "*rag2*$^{-/-}$"). Robust engraftment was observed at the site of injection. All recipient fish demonstrated rapidly growing melanotic tumor masses within 2 weeks (Figure 1g). Because of the invasive properties of the primary *nf1/pten*-mutant melanomas (Figure 1), we also tested the feasibility of their intramuscular transplantation into *rag2*$^{-/-}$ zebrafish, where the tumor cells not only expanded within muscle, but also invaded neighboring tissues such as the ventral fin (Supplementary Figure S6). By contrast, non-

transformed melanocytes (derived from normal pigmented melanocytes within the skin stripes) from *nf1a*$^{+/-}$;*nf1b*$^{-/-}$;*ptena*$^{+/-}$;*ptenb*$^{-/-}$;*p53*$^{M214K/M214K}$ zebrafish failed to engraft in *rag2*$^{-/-}$ zebrafish. Furthermore, although the melanomas arising from the *Tg(mitf:BRAF*^{V600E}*);p53*$^{M214K/M214K}$ zebrafish[24] can be serially transplanted into *rag2*$^{-/-}$ zebrafish, their post-transplantation growth rates were much slower, highlighting the extraordinarily high growth rate *in vivo* of the *nf1/pten*-mutant melanomas.

MEK and PI3K inhibitors lack efficacy against *nf1/pten*-mutant melanomas *in vivo.*

Human *NF1*-mutant melanomas have the worst outcome among all metastatic melanomas[8], and *PTEN*-mutant melanomas are known to be resistant to T-cell mediated immunotherapy such as the immune checkpoint inhibitor[25]. Thus, there is a clear need for effective small molecule inhibitors to overcome the aggressive growth properties of NF1/PTEN-mutant melanoma. Because targeting the RAS-MEK-ERK and PI3K-PTEN-AKT-mTOR signaling pathways might logically affect the growth of *nf1/pten*-mutant melanomas, we first transplanted these melanoma cells into 3-week-old *rag2*$^{-/-}$ zebrafish and treated the recipients with MEK (trametinib or cobimetinb) or pan-PI3K (buparlisib or apitolisib) inhibitors. The *nf1/pten*-mutant melanoma cells grew rapidly in DMSO-treated recipients and progressed from an inoculum of 500 cells to readily detectable pigmented tumors at 4-8 days post-transplantation (Figure 2a). Single-agent treatment with either MEK or PI3K inhibitors from days 2-8 post-transplantation at each of their maximum tolerated dosages (MTDs; Supplementary Figure S7a) did not affect the growth of tumors (Figures 2b and S7b). Even when tumor-bearing recipient fish were treated with a combination of trametinib and buparlisib at their MTDs (Supplementary Figure S7a), tumor growth was only transiently inhibited during treatment, followed by rapid regrowth after drug removal, resulting in the lack of improvement in overall survival (Figure 2d).

Inhibition of mTOR suppresses the growth of *nf1/pten*-mutant melanomas *in vivo.*

To broaden the coverage of candidate pathway inhibitors, we next tested a panel of antitumor drugs targeting the RAS-MEK-ERK and receptor tyrosine kinase-PI3K-AKT-mTOR pathways in our *nf1/pten*-mutant melanoma model by assessing tumor cell growth and overall survival of recipient *rag2*$^{-/-}$ fish after 6 days of treatment (Figures 2, S8 and S9). Among the 14 tested drugs, each at their MTD, only the rapamycin family of mTOR inhibitors (rapalogs) showed selective activity against *nf1/pten*-mutant melanoma *in vivo* as single agents. Interestingly, four different mTOR kinase inhibitors did not show activity against *nf1/pten*-mutant melanomas at their MTD (Supplementary Figure S9). During the 6-day treatment course, sirolimus (rapamycin) clearly suppressed the appearance of detectable tumors, and its inhibition of tumor growth persisted for 1 to 2 weeks post-treatment, in marked contrast to the rapid tumor regrowth in fish treated with MEK and PI3K inhibitors (Figures 2c, 2e, 3 and S10). We also treated *nf1/pten*-mutant melanomas with everolimus and temsirolimus, two FDA-approved analogs of sirolimus. The three rapalogs showed similar abilities to durably inhibit melanoma cell growth (Figures 2c and e), which uniformly translated to improved overall survival, indicating that rapalogs may provide a useful treatment option for these melanomas *in vivo*.

Primary *nf1/pten*-mutant tumors are invariably melanotic, but after serial transplantation, the tumor cells often become amelanotic[26]. In order to track the melanoma cells using EGFP instead of melanin, we bred the *sox10*:EGFP fluorescent zebrafish line into our *nf1/pten*-mutant line to aid in visualization of the transplanted melanoma cells, as they expressed high levels of the neural crest progenitor marker *sox10* (Supplementary Figure S11)[24]. When transplanted into 3-week-old *rag2*$^{-/-}$ zebrafish and treated for 6 days with multiple different inhibitors, the EGFP-expressing amelanotic cells responded poorly to single-agent treatment with either trametinib or buparlisib, had only temporary responses to the trametinib-buparlisib combination, but showed more durable responses to sirolimus and temsirolimus (Supplementary Figure S12). Thus, the

amelanotic melanoma cells appear to respond in a similar fashion to the melanotic melanoma cells, reinforcing the dependence of both subtypes of melanoma on mTOR signaling for malignant cell growth *in vivo*.

Cell growth in *nf1/pten*-mutant melanomas depends on mTOR signaling.

The RAS-MEK-MAPK and PI3K-AKT-mTOR pathways negatively regulate each other, such that a drug-induced blockade of one pathway results in increased activity of the other[27,28]. To test whether these drugs act on the expected pathways in inhibitor-treated *nf1/pten*-mutant melanomas, we analyzed treated tumors by IHC, observing that treatment with the MEK inhibitor trametinib leads to a reduction in pERK levels (Figures 4a and b), as expected; while levels of pAKT and pS6 are increased (Figures 4a, c and d), reflecting the loss of RAS-MEK-MAPK-mediated cross-inhibition of PI3K-AKT-mTOR signaling[28]. Similarly, treatment with the PI3K inhibitor buparlisib led to a reduction in pAKT and pS6 levels, with loss of RAS-MEK-MAPK-mediated cross-inhibition, resulting in increased pERK levels (Figures 4a-d). This concomitant upregulation of an alternative pathway explains why neither buparlisib nor trametinib alone inhibited tumor-cell proliferation (Figures 4a and e). The trametinib-buparlisib combination readily inhibited both the RAS and PI3K pathways, leading to a significant, though modest, decrease in tumor-cell proliferation (Figure 4). Thus, these two pathways appear to function redundantly in driving the proliferation of *nf1/pten*-mutant melanomas. Interestingly, 2 days of sirolimus treatment resulted in undetectable levels of pS6 staining (Figures 4a and d), reflecting mTOR inhibition with transient increase and then sustained loss of pERK levels (Figures 4a, 4b and 5) and suppression of proliferation (Figure 4). Thus, the sustained compensatory upregulation of the ERK pathway induced by buparlisib was not evident when mTOR-mediated phosphorylation was specifically inhibited by sirolimus.

To assess the durability of pathway suppression by inhibitor treatment, we treated *nf1/pten*-mutant-melanoma recipients with the inhibitors for 6 days, then analyzed the tumors after 4 days in the absence of the drugs. Sirolimus led to sustained reductions in pERK, pAKT, pS6, and PCNA levels at 4 days post-treatment (Figures 5a-c), as part of a cytoprotective autophagy stress response (Figure 6a). By contrast, the initial signaling and antiproliferative effects of the trametinib-buparlisib combination (Figure 4) were short-lived, as 4 days after drug removal, the pERK, pAKT, pS6 and PCNA levels were returning to normal (Figure 5). Similar to sirolimus, temsirolimus also induced durable inhibition of pS6 and sustained suppression of pERK, pAKT and tumor proliferation (Supplementary Figure S13). Thus, in contrast to combined inhibition of PI3K and MEK, mTOR inhibition alone leads to the sustained suppression of RAS and PI3K pathways and tumor cell growth in transplanted melanomas.

Co-inhibition of BCL2 and MCL1 synergizes with sirolimus to cause apoptotic cell death *nf1/pten*-mutant melanomas *in vivo*

It is important to emphasize that while either sirolimus or temsirolimus can induce prolonged proliferative arrest based on the absence of PCNA staining, we did not detect cleaved caspase 3 in treated tumor cells (Figures 4a, 5a and S13), indicating that neither agent is cytotoxic as a single agent. To query further the proliferative arrest induced by these rapalogs, we studied the autophagy marker LC3 by IHC. This analysis revealed autophagy not only of the tumor cells by LC3 staining, but also striking levels of autophagy in the brain and liver of the sirolimus-treated animals (Figure 6a). The absence of a cytotoxic effect and initiation of autophagy as a cell survival mechanism would likely limit the therapeutic potential of rapalogs in *nf1/pten*-mutant melanomas. Thus, we analyzed a panel of antitumor drugs to identify those with the potential to synergize with sirolimus by inducing apoptosis, thus converting "cytostatic autophagy" to "cytotoxic autophagy"[29]. This evaluation included MEK inhibitors trametinib and cobimetinib,

the PI3K inhibitors buparlisib and apitolisib, the pan-RAF inhibitor sorafenib, the PARP inhibitor olaparib, the autophagy inhibitor chloroquine, and inhibitors of the BCL2 family of pro-survival proteins including sabutoclax, obatoclax, venetoclax and S63845 (MTD determination see Supplementary Figure S14).

As shown in Supplementary Figure S15, none of the drugs delayed tumor progression when given alone to 3-week-old fish bearing *nf1/pten*-mutant melanomas, and only sirolimus in combination with venetoclax showed overall survival benefit compared to sirolimus alone. In particular, the autophagy inhibitor chloroquine markedly delayed tumor progression when combined with sirolimus, presumably by blocking the ability of the autophagosomes to fuse with lysosomes, thus preventing both tumor and normal cells from accessing the nutrients sequestered in the autophagosome[30-32]. However, its use with sirolimus caused massive post-treatment death of the recipient fish as early as 4 days after drug administration, presumably due to autophagy of normal tissues such as liver (Figures 6 and S15). Thus, we sought to identify drugs that would modify the autophagy response not directly as in the case of chloroquine but selectively by promoting apoptosis.

Pro-survival members of the BCL2 family of proteins are required for the survival of cells undergoing autophagy[33], with tumor cells typically showing greater dependence on these pro-survival effects because of their higher-than-normal expression of BH3-only initiators of apoptosis, leading to an increased propensity to undergo apoptosis through a mechanism called "apoptotic priming"[34]. Thus, since pro-survival BCL2 family proteins are essential in the high-stress environment induced by sirolimus, their inhibition would be expected to induce tumor cells to undergo apoptosis before normal cells[35-38]. Therefore, inhibitors of pro-survival BCL2 family proteins should have a therapeutic index based on synergy with the effects of sirolimus in targeted therapy for "primed" NF1/PTEN-mutant tumor cells, while sparing normal tissues.

To test this hypothesis, we focused on two inhibitors, venetoclax (inhibiting BCL2)[39] and S63845 (inhibiting MCL1)[40]. Interestingly, although venetoclax alone had no effect on tumor growth at a dose of 7.5 μM, its combination with 10 μM sirolimus significantly delayed tumor progression (Figures 6b and c). Similarly, S63845 alone did not affect tumor growth at a dose of 5 μM, but in combination with 10 μM sirolimus, it augmented the growth suppressive effects of sirolimus (Figures 6d and e).

It is known that each member of the pro-survival BCL2 family proteins, including BCL2 and MCL1, can bind and sequester BH3-only proteins independently and thereby prevent these BH3-only proteins from inducing apoptosis by activating BAX and BAK[39]. We previously discovered in vivo synergistic anti-leukemia activity of venetoclax and S63845, as each drug causes marked compensatory upregulation of MCL1 and BCL2 protein levels when used as single agent in zebrafish[41]. Hence, we reasoned that co-inhibition of BCL2 and MCL1 in *nf1/pten*-mutant melanoma cells might produce an even greater synergistic antitumor effect than observed with either inhibitor given individually with sirolimus. Indeed, when we combined 7.5 μM venetoclax and 2.5 μM S63845 with 10 μM sirolimus, we observed greatly enhanced growth suppression of *nf1/pten*-mutant melanoma cells (Figures 6f and g). To determine the basis for this boosted effect, we analyzed the contributions of these three agents to tumor cell proliferation and apoptosis. 7.5 μM venetoclax and 2.5 μM S63845 had no effect on proliferation or apoptosis, while 10 μM sirolimus significantly inhibited proliferation but failed to induce apoptosis (Figures 6h and i). In combination, however, the three drugs effectively inhibited proliferation, and dramatically increased levels of apoptosis (Figures 6h and i). Importantly, the fish tolerated this drug combination without noticeable toxicity. Thus, our results indicate that tumor cells sensitized by sirolimus become more dependent than normal cells on BCL2 and MCL1 for sustained survival, thus increasing their susceptibility to apoptosis in the absence of these key pro-survival proteins.

Co-inhibition of BCL2 and MCL1 synergizes with sirolimus to induce apoptosis in human *NF1/PTEN*-deficient melanoma cells

To validate the efficacy of our three-drug combination, we turned to studies using human NF1/PTEN-deficient melanoma cells. For this purpose, we first evaluated the expression level of neurofibromin and PTEN in a panel of human melanoma cell lines and identified one cell line, WM-3246, that lacked detectable expression of either neurofibromin or PTEN (Figure 7a). Then, using WM-3246 cells, we tested the effects of sirolimus, venetoclax and S63845 on the viability of NF1/PTEN-deficient melanoma cells. As a single agent, sirolimus induced only modest levels of cytostatic growth suppression at concentrations >50 nM (Figures 7b-d). Venetoclax did not produce effects on WM-3246 cell growth at concentrations up to 250 nM, whereas S63845 suppressed cell growth in a dose-dependent manner at doses >5 nM (Figures 7b-c). The greatest impact on cell growth was evident when sirolimus was tested in combination with venetoclax and S63845 (Figures 7c-d); synergy was obtained by isobologram analysis over a range of drug concentrations (Figure 7e), indicating that these cells depend on both BCL2 and MCL1, as well as on mTOR signaling, for cell growth and survival. Western blot analysis showed compensatory upregulation of MCL1 in cells treated with venetoclax (Figure 7f), confirming the molecular basis for the synergy between S63845 and venetoclax in sirolimus-treated WM-3246 cells. Furthermore, cleaved caspase 3 in WM-3246 cells treated with the three-drug combination but not with sirolimus alone (Figure 7g), validating the induction of apoptosis by co-inhibition of BCL2 and MCL1 in sirolimus-sensitized NF1/PTEN-deficient human melanoma cells.

We also tested the three-drug combination identified in our NF1/PTEN-mutant melanoma model in BRAF-mutant melanomas with PTEN-mutations, because BRAF activation by mutation is more prevalent than biallelic inactivating mutations of NF1. Although each of these drugs demonstrated little or no activity as single agents, the three-drug combination showed significant

activity against the BRAF-mutant melanoma cells harboring PTEN-mutation (Supplementary Figure S16). Furthermore, the venetoclax-S63845 combination potentiated melanoma cell killing caused by the BRAFV600E inhibitor darafenib in BRAF-mutant melanoma cells (Supplementary Figure S16), suggesting that co-inhibition of BCL2 and MCL1 as a strategy to enhance the induction of apoptosis has broad utility as a means to potentiate the activity of targeted therapies in disseminated human melanomas.

Discussion

Loss-of-function mutations of the *NF1* tumor suppressor in human melanoma cells were first identified by us and others in the early 1990s[42,43]. The TCGA program subsequently undertook a multiplatform characterization of cutaneous melanoma samples at the DNA, RNA and protein levels, in which *NF1*-mutant melanoma emerged as an important subtype within a genomic classification framework[2]. Although highly useful as a means to identify cooperative molecular aberrations that might serve as druggable targets or predictive biomarkers, this genomic approach did not suggest a therapeutic strategy for tumors linked to *NF1*-loss. Using a zebrafish experimental system that models human NF1-mutant melanomas, we show that activation of both the RAS and PI3K pathways in a background of *pten*-loss is required to initiate melanomas in *nf1*-deficient animals. However, the RAS and PI3K pathways function redundantly in tumor maintenance, due to compensatory upregulation of either pathway when the other is inhibited (Figures 4 and 5). Even simultaneous inhibition of both pathways only transiently inhibited the growth of *nf1/pten*-mutant melanomas, such that the overall survival of tumor-bearing fish was unaffected (Figures 2, S7 and S10). This result contrasts with findings in basal-like breast cancer cell lines, in which the combination of MEK and PI3K inhibitors produced cytotoxic antitumor effects[44].

Given the superiority of sirolimus in suppressing the growth of transplanted *nf1/pten*-mutant melanomas while inducing autophagy in normal tissues, we faced a major challenge: to identify drugs that could selectively cause apoptosis in sirolimus-sensitized melanoma cells. Such studies require an animal model that allows one to simultaneously assess both antitumor effects and toxicity to normal tissues, a criterion that was readily met by our zebrafish model. Indeed, while the antitumor response of *nf1/pten*-mutant melanomas to the combination of sirolimus and chloroquine initially appeared promising, the treated fish died due to toxicity to normal tissues (Supplementary Figure S15), illustrating the importance of analyzing this drug combination in an

in vivo model system. By contrast, the combination of sirolimus with inhibitors of the anti-apoptotic proteins BCL2 (venetoclax) and MCL1 (S63845) was both well tolerated by normal tissues and highly active in inducing apoptosis in tumor cells (Figures 6, 7 and S15). This selectivity apparently results from the fact that the malignant cells are "primed" to undergo apoptosis, while normal cells do not harbor the same levels of upregulation of BH3-only death proteins and can survive and maintain mitochondrial integrity despite the simultaneous inhibition of two major pro-survival proteins.

Our results underscore the advantages of using a reliable in vivo preclinical model to analyze the effects of simultaneously inhibiting multiple pathways with small-molecule drugs. Given its greater efficiency and lower costs compared to murine models, our zebrafish experimental system appears ideal for pursuing additional classes of pathway inhibitors in *NF1/PTEN*-mutant melanomas, as single agents and in combination, to define their clinical translational potential. Thus, the three-drug combination of sirolimus, venetoclax and S63845 is well tolerated at effective dosages in vivo and shows activity against human as well as zebrafish NF1/PTEN-deficient melanoma cells, providing preclinical evidence justifying an early stage clinical trial in patients with melanomas of this high-risk genomic subtype. Notably, the three-drug combination identified in our NF1/PTEN-mutant melanoma model also showed anti-melanoma activity in BRAF-mutant melanoma cells harboring PTEN-mutation (Supplementary Figure S16). Furthermore, the venetoclax-S63845 combination potentiated melanoma cell killing caused by the BRAFV600E inhibitor darafenib in BRAF-mutant melanoma cells (Supplementary Figure S16). Thus the potentiation of apoptosis induced by co-inhibition of BCL2 and MCL1 is a strategy with wide applicability to enhance the anti-melanoma activity by targeted therapies in malignant melanoma.

Materials and Methods

Zebrafish

Zebrafish experiments and animal husbandry were performed in accordance with Dana-Farber Cancer Institute IACUC-approved protocol #02-107.

Melanoma tumor watch

nf1a$^{+/-}$;*nf1b*$^{+/-}$;*ptena*$^{+/-}$;*ptenb*$^{+/-}$;*p53*$^{+/M214K}$ mutant zebrafish were incrossed, and offspring were monitored every week, starting at 3 weeks, for hyperpigmented cell masses indicative of melanoma tumors. Once a hyperpigmented cell mass was identified, the individual fish was separated and carefully monitored weekly for at least 3 weeks for tumor progression. Only fish with expanding hyperpigmented cell masses were scored as tumor fish and analyzed further by H&E staining and immunohistochemical assays. All fish were genotyped for *nf1a*, *nf1b*, *ptena*, *ptenb* and *p53* at the age of 6 weeks. The exact sample size (n) for each experimental group is indicated in the figures.

Tumor cell transplantation

rag2^{E450fs}*(casper)* (*rag2*$^{-/-}$*)* zebrafish were anaesthetized with 0.003% tricaine (Sigma-Aldrich, St. Louis, MO) and positioned on a 10-cm Petri dish coated with 1% agarose. Primary and serially-passaged tumors derived from *nf1a*$^{+/-}$;*nf1b*$^{-/-}$;*ptena*$^{+/-}$;*ptenb*$^{-/-}$;*p53*$^{M214K\ /M214K}$ and *nf1a*$^{+/-}$;*nf1b*$^{-/-}$;*ptena*$^{+/-}$;*ptenb*$^{-/-}$;*p53*$^{M214K/M214K}$;*Tg(sox10:EGFP)* zebrafish lines were excised from tumor-bearing fish and mechanically dissociated with a razor blade in 0.9X PBS + 5% FBS (Life Technologies, Carlsbad, CA) at room temperature. Collected cell suspension was filtered through a 40-μm cell strainer (Falcon, Corning, NY) and resuspended in 0.9X PBS + 5% FBS. For the intraperitoneal and intramuscular transplantation into 3- to 4-month-old adult *rag2*$^{-/-}$ fish, a

26s/2"/2 Hamilton 80300 syringe (Hamilton, Reno, NV) was used[23]. For the intraperitoneal transplantation into 3-week-old juvenile *rag2*$^{-/-}$ fish, cell suspensions were loaded into borosilicate glass capillary needles (1 mm o.d. × 0.78 mm i.d.; Harvard Apparatus, Holliston, MA), and the injections were performed with a Pneumatic Picopump and a manipulator (WPI, Sarasota, FL) [45].

Cell culture

Melanoma cell lines Mewo, WM-3246, WM-3622, WM-3629, WM-3670 and WM-3918 were purchased from Rockland (Rockland Immunochemicals Inc, Limerick, PA), and maintained in Dulbecco's modified Eagle's medium supplemented with 10% FBS, L-glutamine, and penicillin/streptomycin. Melanoma cell lines COLO829 and C32 were purchased from ATCC (ATCC, Manassas, VA) and maintained according to the provided Culture Methods. HEK-293T cells were purchased from ATCC, and maintained in Dulbecco's modified Eagle's medium supplemented with 10% FBS, L-glutamine, and penicillin/streptomycin. Jurkart cells were maintained in RPMI-1640 medium supplemented with 10% FBS, L-glutamine, and penicillin/streptomycin. The identity of cell lines used in this study was verified by short tandem repeat analysis using the PowerPlex 1.2 system (Promega). The cell lines were tested for mycoplasma contamination using MycoAlert Mycoplasma Detection Kits (Lonza).

Statistical analysis

Statistical analysis was performed with Prism 5 software (GraphPad). Kaplan-Meier methods and the log-rank test were applied to assess the rate of tumor growth in Figure 1 and S1, and tumor progression in Figures 2, 6, S7, S8, S9, S10 and S15. The quantitative data in Figures 3, 4, 5 and S12 are reported as median values. A Mann-Whitney test with confidence intervals of 95% was used for the analyses in Figures 3, 4, 5, 6 and S12.

References and Notes

1 Siegel, R. L., Miller, K. D. & Jemal, A. Cancer statistics, 2020. *CA: A Cancer Journal for Clinicians* **70**, 7-30, doi:10.3322/caac.21590 (2020).

2 Akbani, R. *et al.* Genomic Classification of Cutaneous Melanoma. *Cell* **161**, 1681-1696, doi:http://dx.doi.org/10.1016/j.cell.2015.05.044 (2015).

3 Maertens, O. *et al.* Elucidating Distinct Roles for NF1 in Melanomagenesis. *Cancer Discovery* **3**, 338-349, doi:10.1158/2159-8290.cd-12-0313 (2013).

4 Whittaker, S. R. *et al.* A Genome-Scale RNA Interference Screen Implicates NF1 Loss in Resistance to RAF Inhibition. *Cancer Discovery* **3**, 350-362, doi:10.1158/2159-8290.cd-12-0470 (2013).

5 Krauthammer, M. *et al.* Exome sequencing identifies recurrent mutations in NF1 and RASopathy genes in sun-exposed melanomas. *Nat Genet* **47**, 996-1002, doi:10.1038/ng.3361 http://www.nature.com/ng/journal/v47/n9/abs/ng.3361.html#supplementary-information (2015).

6 Hayward, N. K. *et al.* Whole-genome landscapes of major melanoma subtypes. *Nature* **545**, 175-180, doi:10.1038/nature22071 (2017).

7 Maertens, O. & Cichowski, K. An expanding role for RAS GTPase activating proteins (RAS GAPs) in cancer. *Advances in Biological Regulation* **55**, 1-14, doi:http://dx.doi.org/10.1016/j.jbior.2014.04.002 (2014).

8 Cirenajwis, H. *et al.* NF1-mutated melanoma tumors harbor distinct clinical and biological characteristics. *Molecular oncology* **11**, 438-451, doi:10.1002/1878-0261.12050 (2017).

9 Kuzu, O. F., Nguyen, F. D., Noory, M. A. & Sharma, A. Current State of Animal (Mouse) Modeling in Melanoma Research. *Cancer growth and metastasis* **8**, 81-94, doi:10.4137/cgm.s21214 (2015).

10 Kaufman, C. K. Zebrafish Melanoma. *Advances in experimental medicine and biology* **916**, 439-450, doi:10.1007/978-3-319-30654-4_19 (2016).

11 Hodis, E. *et al.* A Landscape of Driver Mutations in Melanoma. *Cell* **150**, 251-263, doi:http://dx.doi.org/10.1016/j.cell.2012.06.024 (2012).

12 De Raedt, T. *et al.* PRC2 loss amplifies Ras-driven transcription and confers sensitivity to BRD4-based therapies. *Nature* **514**, 247-251, doi:10.1038/nature13561 http://www.nature.com/nature/journal/v514/n7521/abs/nature13561.html#supplementary-information (2014).

13 Shin, J. *et al.* Zebrafish neurofibromatosis type 1 genes have redundant functions in tumorigenesis and embryonic development. *Disease Models & Mechanisms* **5**, 881-894, doi:10.1242/dmm.009779 (2012).

14 Garman, B. *et al.* Genetic and Genomic Characterization of 462 Melanoma Patient-Derived Xenografts, Tumor Biopsies, and Cell Lines. *Cell reports* **21**, 1936-1952, doi:10.1016/j.celrep.2017.10.052 (2017).

15 Mar, V. J. *et al.* BRAF/NRAS wild-type melanomas have a high mutation load correlating with histologic and molecular signatures of UV damage. *Clinical cancer research : an official journal of the American Association for Cancer Research* **19**, 4589-4598, doi:10.1158/1078-0432.ccr-13-0398 (2013).

16 Gutierrez, A. *et al.* Pten mediates Myc oncogene dependence in a conditional zebrafish model of T cell acute lymphoblastic leukemia. *The Journal of Experimental Medicine* **208**, 1595-1603, doi:10.1084/jem.20101691 (2011).

17 Faucherre, A., Taylor, G. S., Overvoorde, J., Dixon, J. E. & Hertog, J. d. Zebrafish pten genes have overlapping and non-redundant functions in tumorigenesis and embryonic development. *Oncogene* **27**, 1079-1086, doi:http://www.nature.com/onc/journal/v27/n8/suppinfo/1210730s1.html (2007).

18 Patton, E. *et al.* BRAF mutations are sufficient to promote nevi formation and cooperate with p53 in the genesis of melanoma. *Curr Biol* **15**, 249-254 (2005).
19 Dovey, M., White, R. M. & Zon, L. I. Oncogenic NRAS Cooperates with p53 Loss to Generate Melanoma in Zebrafish. *Zebrafish* **6**, 397-404, doi:10.1089/zeb.2009.0606 (2009).
20 Ceol, C. J. *et al.* The histone methyltransferase SETDB1 is recurrently amplified in melanoma and accelerates its onset. *Nature* **471**, 513-517, doi:http://www.nature.com/nature/journal/v471/n7339/abs/10.1038-nature09806-unlocked.html#supplementary-information (2011).
21 Lister, J. A. *et al.* A conditional zebrafish MITF mutation reveals MITF levels are critical for melanoma promotion vs. regression in vivo. *The Journal of investigative dermatology* **134**, 133-140, doi:10.1038/jid.2013.293 (2014).
22 Cully, M., You, H., Levine, A. J. & Mak, T. W. Beyond PTEN mutations: the PI3K pathway as an integrator of multiple inputs during tumorigenesis. *Nat Rev Cancer* **6**, 184-192 (2006).
23 Tang, Q. *et al.* Imaging tumour cell heterogeneity following cell transplantation into optically clear immune-deficient zebrafish. *Nat Commun* **7**, doi:10.1038/ncomms10358 (2016).
24 Kaufman, C. K. *et al.* A zebrafish melanoma model reveals emergence of neural crest identity during melanoma initiation. *Science* **351**, doi:10.1126/science.aad2197 (2016).
25 Peng, W. *et al.* Loss of PTEN Promotes Resistance to T Cell-Mediated Immunotherapy. *Cancer Discov* **6**, 202-216, doi:10.1158/2159-8290.cd-15-0283 (2016).
26 Chen, K. G. *et al.* Influence of melanosome dynamics on melanoma drug sensitivity. *J Natl Cancer Inst* **101**, 1259-1271, doi:10.1093/jnci/djp259 (2009).
27 Yang, S., Xiao, X., Meng, X. & Leslie, K. K. A mechanism for synergy with combined mTOR and PI3 kinase inhibitors. *PLoS One* **6**, e26343, doi:10.1371/journal.pone.0026343 (2011).
28 Mendoza, M. C., Er, E. E. & Blenis, J. The Ras-ERK and PI3K-mTOR pathways: cross-talk and compensation. *Trends in Biochemical Sciences* **36**, 320-328, doi:http://dx.doi.org/10.1016/j.tibs.2011.03.006 (2011).
29 Sharma, K., Le, N., Alotaibi, M. & Gewirtz, D. A. Cytotoxic autophagy in cancer therapy. *International journal of molecular sciences* **15**, 10034-10051, doi:10.3390/ijms150610034 (2014).
30 Kaneko, M. *et al.* Temsirolimus and chloroquine cooperatively exhibit a potent antitumor effect against colorectal cancer cells. *Journal of cancer research and clinical oncology* **140**, 769-781, doi:10.1007/s00432-014-1628-0 (2014).
31 Rangwala, R. *et al.* Combined MTOR and autophagy inhibition: phase I trial of hydroxychloroquine and temsirolimus in patients with advanced solid tumors and melanoma. *Autophagy* **10**, 1391-1402, doi:10.4161/auto.29119 (2014).
32 Avniel-Polak, S. *et al.* Abrogation of Autophagy by Chloroquine Alone or in Combination with mTOR Inhibitors Induces Apoptosis in Neuroendocrine Tumor Cells. *Neuroendocrinology* **103**, 724-737, doi:10.1159/000442589 (2016).
33 Macintosh, R. L. & Ryan, K. M. Autophagy in tumour cell death. *Seminars in cancer biology* **23**, 344-351, doi:10.1016/j.semcancer.2013.05.006 (2013).
34 Potter, D. S. & Letai, A. To Prime, or Not to Prime: That Is the Question. *Cold Spring Harbor symposia on quantitative biology* **81**, 131-140, doi:10.1101/sqb.2016.81.030841 (2016).
35 McGill, G. G. *et al.* Bcl2 regulation by the melanocyte master regulator Mitf modulates lineage survival and melanoma cell viability. *Cell* **109**, 707-718 (2002).

36 Mohana-Kumaran, N., Hill, D. S., Allen, J. D. & Haass, N. K. Targeting the intrinsic apoptosis pathway as a strategy for melanoma therapy. *Pigment cell & melanoma research* **27**, 525-539, doi:10.1111/pcmr.12242 (2014).
37 Lam, L. T. *et al.* A microRNA screen to identify modulators of sensitivity to BCL2 inhibitor ABT-263 (navitoclax). *Molecular cancer therapeutics* **9**, 2943-2950, doi:10.1158/1535-7163.mct-10-0427 (2010).
38 Mukherjee, N., Schwan, J. V., Fujita, M., Norris, D. A. & Shellman, Y. G. Alternative Treatments For Melanoma: Targeting BCL-2 Family Members to De-Bulk and Kill Cancer Stem Cells. *The Journal of investigative dermatology* **135**, 2155-2161, doi:10.1038/jid.2015.145 (2015).
39 Leverson, J. D. *et al.* Found in Translation: How Preclinical Research Is Guiding the Clinical Development of the BCL2-Selective Inhibitor Venetoclax. *Cancer Discov* **7**, 1376-1393, doi:10.1158/2159-8290.cd-17-0797 (2017).
40 Kotschy, A. *et al.* The MCL1 inhibitor S63845 is tolerable and effective in diverse cancer models. *Nature* **538**, 477-482, doi:10.1038/nature19830 (2016).
41 Li, Z., He, S. & Look, A. T. The MCL1-specific inhibitor S63845 acts synergistically with venetoclax/ABT-199 to induce apoptosis in T-cell acute lymphoblastic leukemia cells. *Leukemia* **33**, 262-266, doi:10.1038/s41375-018-0201-2 (2019).
42 Andersen, L. B. *et al.* Mutations in the neurofibromatosis 1 gene in sporadic malignant melanoma cell lines. *Nat Genet* **3**, 118-121 (1993).
43 Johnson, M. R., Look, A. T., DeClue, J. E., Valentine, M. B. & Lowy, D. R. Inactivation of the NF1 gene in human melanoma and neuroblastoma cell lines without impaired regulation of GTP.Ras. *Proceedings of the National Academy of Sciences* **90**, 5539-5543 (1993).
44 Hoeflich, K. P. *et al.* In vivo Antitumor Activity of MEK and Phosphatidylinositol 3-Kinase Inhibitors in Basal-Like Breast Cancer Models. *Clinical Cancer Research* **15**, 4649-4664, doi:10.1158/1078-0432.ccr-09-0317 (2009).
45 He, S. *et al.* Neutrophil-mediated experimental metastasis is enhanced by VEGFR inhibition in a zebrafish xenograft model. *The Journal of Pathology* **227**, 431-445, doi:10.1002/path.4013 (2012).

Acknowledgments

We would like to thank John Gilbert for critical review of the manuscript and editorial suggestions; Kassandra Bacon and Daniel Debiasi for zebrafish husbandry; Jeoren den Hertog, Alejandro Gutierrez and David M. Langenau for providing zebrafish lines; Yi Zhou and Andrew Hong for stimulating suggestions; Christine L. Unitt, Benjamin Ferland and Dana-Farber/Harvard Cancer Center Research Pathology Core for technical support. This study was funded by Melanoma Research Alliance award #509233.

Figures and Tables

Figure 1: *nf1a*$^{+/-}$;*nf1b*$^{-/-}$;*ptena*$^{+/-}$;*ptenb*$^{-/-}$;*p53*$^{M214K/M214K}$ zebrafish spontaneously develop melanomas with rapid growth.

(a) Representative 16-week-old *nf1a*$^{+/-}$;*nf1b*$^{-/-}$;*ptena*$^{+/-}$;*ptenb*$^{-/-}$;*p53*$^{M214K/M214K}$ zebrafish with one spontaneous melanoma (indicated by arrow). (b) Hematoxylin and eosin (H&E) staining of the melanoma tumor shown in panel a (5x magnification, scale bar = 200 μm). (c) Melanoma tumor cells from the black box in panel B, magnified 100X. (d) Melanoma tumor cells that have invaded into the dorsal muscle from the white box in panel B, magnified 100X. (e) Cumulative frequency of spontaneous melanomas arising in zebrafish with the indicated genotypes (generated by the inbreeding of the *nf1a*$^{+/-}$;*nf1b*$^{-/-}$;*ptena*$^{+/-}$;*ptenb*$^{-/-}$;*p53*$^{M214K/M214K}$ line, $p < 0.0001$, log-rank test). (f) Immunohistochemical analysis of melanoma tumor sections using antibodies to detect phosphorylated ERK1/2 (pERK), phosphorylated AKT (pAKT), phosphorylated S6 (pS6), proliferating cell nuclear antigen (PCNA) and cleaved caspase 3 (CC3) (63x magnification, scale bar = 20μm). The percentage of PCNA+ cells was determined by manually counting positive and negative melanoma cells in one representative high-power field (150 to 200 cells per field) within three independent tumor samples. (g) Pigmented *nf1/pten*-mutant melanoma cells were transplanted intraperitoneally into adult *rag2*$^{-/-}$ Casper zebrafish. The implanted melanoma cells (left panel, arrow) grew rapidly into secondary tumors (within 2 weeks; right panel).

Figure 2: mTOR inhibitors achieve a durable antitumor effect in *nf1/pten*-mutant melanoma.

(a) Schematic of the melanoma tumor transplantation assay. (b, c) Transplanted *nf1/pten*-mutant melanoma tumor cells were monitored daily in 3-week-old *rag2*$^{-/-}$ recipient zebrafish treated with DMSO (CTR; n=12), 80 nM trametinib (n=11), 2 μM buparlisib (n=11), or the combination of 80

nM trametinib and 2 μM buparlisib (n=12) for 6 days. Kaplan-Meier curves for progression-free survival (PFS, panel b) and overall survival (OS, panel c) are shown. Statistical analyses were performed by log-rank test, comparing drug-treated with DMSO-treated zebrafish. (d, e) Transplanted *nf1/pten*-mutant melanoma tumor cells were monitored daily in 3-week-old *rag2*$^{-/-}$ recipient zebrafish treated with DMSO (CTR; n=12, same values as in panels b, c), 20 μM sirolimus (n=12), 20 μM everolimus (n=11) or 40 μM temsirolimus (n=11) for 6 days. Kaplan-Meier curves are shown, with statistical analyses performed as in panels B, C. For all experiments involving drug treatments, drugs were replenished every 2 days during the 6-day course of treatment (black arrows).

Figure 3: Sirolimus, but not trametinib or buparlisib, prevents rapid relapse of *nf1/pten*-mutant melanoma following treatment. Three-week-old *rag2*$^{-/-}$ zebrafish transplanted with pigmented *nf1/pten*-mutant melanoma cells were treated for 6 days with DMSO, 80 nM trametinib, 2 μM buparlisib, the combination of 80 nM trametinib and 2 μM buparlisib, or 20 μM sirolimus. (a, c, e, g, and i) Representative zebrafish at the end of the 6-day drug treatment. (b, d, f, h, and j) Representative zebrafish at 4 days following the end of drug treatment. (k) Quantification of melanotic *nf1/pten*-mutant tumor-cell area at the end of the 6-day course of drug treatment (left), and 4 days later (right). ns $p>0.05$, *$p<0.05$, **$p<0.01$, ***$p<0.001$ by two-tailed, unpaired t-test. Scale bar = 1mm.

Figure 4: Sirolimus strongly inhibits proliferation in *nf1/pten*-mutant melanomas. (a) Representative tissue sections from a transplanted *nf1/pten*-mutant melanoma tumor after 2 days of treatment with DMSO (CTR), 80 nM trametinib, 2 μM buparlisib, the combination of 80 nM trametinib and 2 μM buparlisib, or 20 μM sirolimus. Sections were immunostained using antibodies to detect pERK, pAKT, pS6, PCNA, and cleaved caspase-3 (CC3). pERK-, pAKT-

and pS6-positive tumor areas, as well as PCNA-positive nuclei, are quantified post-treatment in panels b-e. "T+B" refers to trametinib plus buparlisib. ns $p>0.05$, * $p<0.05$, ** $p<0.01$ by Mann-Whitney test. Scale bar = 20 μm.

Figure 5: Sirolimus induces a durable cytostatic effect in *nf1/pten*-mutant melanomas. (a) Representative tissue sections from a transplanted *nf1/pten*-mutant melanoma tumor at 4 days after a 6-day drug treatment with DMSO (CTR), 80 nM trametinib, 2 μM buparlisib, the combination of 80 nM trametinib and 2 μM buparlisib, or 20 μM sirolimus. Sections were immunostained using antibodies to detect pERK, pAKT, pS6, PCNA, and CC3. pERK-, pAKT- and pS6-positive tumor areas, as well as PCNA-positive nuclei, are quantified in panels b-e. "T+B" refers to trametinib plus buparlisib. ns $p>0.05$, * $p<0.05$, ** $p<0.01$ by Mann-Whitney test. Scale bar = 20 μm.

Figure 6: **Sirolimus synergizes with venetoclax and S63845 to suppress *nf1/pten*-mutant melanoma tumor growth and extend the survival of tumor-bearing zebrafish.** (a) Representative sagittal tissue sections from a transplanted *nf1/pten*-mutant melanoma tumor treated for 2 days with the indicated drugs. Sections were immunostained with antibodies to detect LC3A/B. *Left panels*: E=eye, B=brain, G=gut, K=kidney, L=liver, S=swim bladder, T=tumor. *Right panels*: 63X magnification of tumor cells from the small black boxes in left panels. (b-g) Transplanted *nf1/pten*-mutant melanoma tumor cells were monitored daily in 3-week-old *rag2*$^{-/-}$ recipient zebrafish treated with DMSO (CTR), venetoclax, S63845, sirolimus, or the drug combinations (n=11 or 12 for each curve; doses as indicated). Kaplan-Meier curves for PFS (panels b, d and f) and OS (panels c, e and g) were compared using a log-rank test. Drugs were refreshed every 2 days during the 6-day course of treatment, as indicated by black arrows. (h) Representative tissue sections from transplanted *nf1/pten*-mutant melanoma tumors treated for

2 days with DMSO (CTR), 7.5 μM venetoclax and 2.5 μM S63845, 10 μM sirolimus, and the three-drug combination. Sections were immunostained using antibodies to detect PCNA and CC3 and quantified in (i). ns $p>0.05$, ***$p<0.0001$ by Mann-Whitney test. Scale bars = 20 μm.

Figure 7: Venetoclax and S63845 synergize with sirolimus to induce apoptosis in human *NF1/PTEN*-deficient melanoma cells. (a) Western blots for NF1 and PTEN in a panel of human melanoma cell lines. HEK293 and Jurkart cells were included as positive and negative controls. The levels of total ERK1/2 expression serve as the loading control. (b) Relative cell viability of WM-3246 cells (Cell Titer Glo assay) upon treatment with sirolimus, venetoclax or S63845 for 6 days. Mean ± s.d. values. (c) Relative cell viability of WM-3246 cells (Cell Titer Glo assay) upon treatment with the combination of sirolimus, venetoclax and S63845 for 6 days. Mean ± s.d. values. (d) WM-3246 cell growth kinetics after treatment with the combination of sirolimus, venetoclax and S63845 (for doses see panel c). Mean ± s.d. values. (e) Synergistic effects of venetoclax and S63845 on suppression of sirolimus-sensitized WM-3246 cells were analyzed by isobologram analysis. (f) Western blots for BCL2, BCLXL and MCL1 in WM-3246 cells treated with venetoclax or S63845 for 24 hours. (g) Western blots for cleaved caspase-3 in WM-3246 cells treated with the combination of sirolimus, venetoclax and S63845.

Supplementary Materials

Supplementary Figure 1: Cumulative frequency of tumor development in fish with the indicated genotypes. Malignant peripheral nerve sheath tumors (MPNSTs) comprise the majority of tumors; high grade gliomas are indicated by red arrows with the single black arrow indicating a spontaneous melanoma.

Supplementary Figure 2: Sections from a spontaneous melanoma from a 20-week-old *nf1a*$^{+/-}$;*nf1b*$^{-/-}$;*ptena*$^{+/-}$;*ptenb*$^{-/-}$;*p53*$^{+/M214K}$ zebrafish were stained for H&E, pERK, pAKT, pS6, and PCNA (63x magnification, Scale bar = 20 μm).

Supplementary Figure 3: DNA PCR of *nf1a* and *ptena* genes were performed from two pairs of independent melanoma tumors (T1 and T2) and the corresponding adjacent non-tumor muscle tissue (A1 and A2). The PCR products were then cut with restriction enzymes that only digests the wild-type allele but not the mutant allele (DdeI for *nf1a* and RsaI for *ptena*). Electrophoresis was performed using 3% MetaPhor agarose. The results showed that the wild-type allele of each gene is retained by the tumor cells.

Supplementary Figure 4: Amino acid sequence alignment of human and zebrafish BRAF (a) and NRAS (b). The sites of BRAF codons V600, and NRAS codons G12 and Q61, are highlighted by red boxes.

Supplementary Figure 5: Representative sequencing chromatograms of zebrafish codons, shown are *braf* codon V610, and *nras* codons G12 and Q61 from genomic DNA isolated from a melanoma tumor (bottom) and matched tumor-free tail fin (top).

Supplementary Figure 6: Rapid growth of *nf1/pten*-mutant melanoma following intramuscular engraftment into adult *rag2*$^{-/-}$ Casper zebrafish. The implanted melanoma cells (a, indicated by the arrow) grew aggressively into secondary tumors within 2 weeks (b).

Supplementary Figure 7: (a) Dose matrices were generated to assess the tolerability of 3-week-old zebrafish to MEK and PI3K inhibitors. Each matrix sampled mixtures of 2 serially diluted

single-agent concentrations. Three 3-week-old wild-type zebrafish were independently treated with each mixture for 7 days, with drug refreshments at days 2 and 4. The numbers of fish surviving the treatment was measured at the end of day 7. (b) Transplanted *nf1/pten*-mutant melanoma tumor cells were monitored daily in 3-week-old *rag2*$^{-/-}$ recipient zebrafish treated with DMSO (CTR; n=12), 1 μM cobimetinib (n=11) and 5 μM apitolisib (n=11) for 20 days. Kaplan-Meier curves for PFS (left) and OS (right) were compared using a log-rank test.

Supplementary Figure 8: Transplanted *nf1/pten*-mutant melanoma cells were monitored daily in 3-week-old *rag2*$^{-/-}$ recipient zebrafish treated with DMSO (CTR) or selected drugs (n=11 or 12 for each curve). Kaplan-Meier curves for progression-free (left) or overall (right) survival were compared with a log-rank test.

Supplementary Figure 9: Transplanted *nf1/pten*-mutant melanoma cells were monitored daily in 3-week-old *rag2*$^{-/-}$ recipient zebrafish treated with DMSO (CTR) or selected mTOR inhibitors (n=11 or 12 for each curve). Kaplan-Meier curves for progression-free (left) or overall (right) survival were compared with a log-rank test.

Supplementary Figure 10: Transplanted *nf1/pten*-mutant melanoma tumor cells were monitored daily in 3-week-old *rag2*$^{-/-}$ recipient zebrafish treated with DMSO (CTR; n=12), 80 nM trametinib (n=11), 2 μM buparlisib (n=12), the combination of 80 nM trametinib and 2 μM buparlisib (n=11), or 20 μM sirolimus (n=12) for 15 days. Kaplan-Meier curves for progression-free (left) or overall (right) survival were compared with a log-rank test (ns $p>0.05$, *$p<0.05$, **$p<0.01$, ***$p<0.001$).

Supplementary Figure 11: Representative tissue section from a transplanted melanoma tumor derived from *nf1a*$^{+/-}$;*nf1b*$^{-/-}$;*ptena*$^{+/-}$;*ptenb*$^{-/-}$;*p53*$^{M214K/M214K}$;*Tg(sox10:EGFP)* zebrafish immunostained with an antibody to GFP. Within the amelanotic tumor mass, a GFP-expressing, melanin-positive melanoma cell is indicated by the arrow. Scale bar = 20μm.

Supplementary Figure 12: **mTOR inhibitors sirolimus and temsirolimus produce a durable antitumor effect on amelanotic *nf1/pten*-mutant melanoma cells.** (a) EGFP-positive amelanotic melanoma cells were isolated from *nf1a*$^{+/-}$;*nf1b*$^{-/-}$;*ptena*$^{+/-}$;*ptenb*$^{-/-}$;*p53*$^{M214K/M214K}$;*sox10:EGFP* zebrafish and injected intraperitoneally into 3-week-old *rag2*$^{-/-}$ zebrafish. Starting at 2 days post-transplantation, the recipient fish were treated with DMSO (CTR), 80 nM trametinib, 2 μM buparlisib, the combination of 80 nM trametinib and 2 μM buparlisib, 20 μM sirolimus, or 40 μM temsirolimus for 6 days. EGFP-expressing tumors were photographed at 4 days post-treatment. The EGFP-expressing area appears as green while the autofluorescence in the gastrointestinal tract appears as yellow. Scale bar = 1 mm. (b) Quantification of the area of EGFP tumor fluorescence immediately after the 6-day course of drug treatment (left) and 4 days later (right). "T+B" refers to trametinib plus buparlisib. ns $p>0.05$, *$p<0.05$, **$p<0.01$, ***$p<0.001$ by two-tailed unpaired t-test.

Supplementary Figure 13: Representative tissue sections from a transplanted *nf1/pten*-mutant melanoma at 4 days after a 6-day drug treatment with DMSO (CTR) and 40 μM temsirolimus. Sections were immunostained with antibodies to detect pERK, pAKT, pS6, PCNA and CC3.

Supplementary Figure 14: Dose matrices were generated to assess the tolerability of 3-week-old zebrafish to sirolimus combined with the indicated drugs. Each matrix sampled mixtures of 2 serially diluted single-agent concentrations. Three 3-week old wild-type zebrafish were

739 independently treated with each mixture for 7 days, with drug replenishment at days 2 and 4. The
740 numbers of fish surviving the treatment was measured at the end of day 7.
741
742 **Supplementary Figure 15**: Three-week-old *rag2*$^{-/-}$ recipient zebrafish were transplanted with
743 *nf1/pten*-mutant melanoma cells and treated with selected drugs as single agents or in
744 combination with 5 μM sirolimus (n=11 or 12 for each curve). Kaplan-Meier curves for
745 progression-free (left) or overall (right) survival were compared with a log-rank test. Drugs were
746 replenished every 2 days during the 6-day course of treatment (black arrows).
747
748 **Supplementary Figure 16**: (a) Venetoclax and S63845 synergize with sirolimus to suppress
749 human melanoma cells harboring BRAFV600E and PTEN mutations. Relative cell viability of
750 COLO829 and C32 cells (Cell Titer Glo assay) upon treatment with the combination of sirolimus,
751 venetoclax and S63845 for 3 days. Mean ± s.d. values. (b) Venetoclax and S63845 synergize
752 with dabrafenib to kill BRAF-mutant melanoma cells. Relative cell viability of C32 cells (Cell
753 Titer Glo assay) upon treatment with the combination of dabrafenib, venetoclax and S63845 for 3
754 days. Mean ± s.d. values.
755

Supplementary Material and Methods

DNA extraction, PCR and sequencing

From each *nf1a*$^{+/-}$;*nf1b*$^{-/-}$;*ptena*$^{+/-}$;*ptenb*$^{-/-}$;*p53*$^{M214K/M214K}$ fish, the melanoma tumor and the tumor-free tail fin were excised, and genomic DNA was extracted with 30 µL QuickExtract DNA Extraction Solution (Epicentre, Madison, WI) according to the manufacturer's instructions. PCR reactions were performed in a 25 µL volume consisting of 4 µL genomic DNA, 1.4 µL 2.5 mM dNTP (Invitrogen, Carlsbad, CA), 0.16 µL SuperTaq enzyme (NEB, New England Biolabs, Ipswich, MA), 2.5 µL 10x SuperTaq buffer (NEB) and 1.4 µL 10 µM primer mix. Cycling parameters were 1) 94°C for 2 min, 2) 40 cycles at 94°C for 30 sec, annealing (temperature depends on primer sets, see below) for 30 sec, and elongation at 72°C for 30 sec, and 3) final elongation for 5 min at 72°C. PCR primer sequences and annealing temperatures were as follow: *nf1a* forward, 5'-GGTGTGTATGTAAATGGGCTCAATG-3' and reverse 5'-TACAGTTTCCATAAAACCTGACATTTC-3' (62°C); *ptena* forward, 5'-TTGCCATGGGCTTTCCAGCCGTA-3' and reverse 5'-CCACGTTGACTTACCGGACAACGTCA-3' (53°C); *brafV610* forward, 5'-ATTAGCCGTAACATCACTTCTCTAG-3' and reverse 5'-ATGTAAGATGTGTTCCTTCACTCAC-3' (53°C); *nrasG12* forward, 5'-GCTTACTCTCTGTCTTTAATTAC-3' and reverse 5'- AAGTATAGTAAATTTCCTCAT-3' (53°C); *nrasQ61* forward, 5'-GTGGCAATCTTGTCTTTC-3' and reverse 5'-CTGCTCTCAGACCTGTAC-3' (60°C). Sequencing of the PCR reaction products were performed by Genewiz (Cambridge, MA).

Immunohistochemistry

Zebrafish were euthanized in tricaine anesthetic, fixed in 4% paraformaldehyde at 4°C for 2 days, and decalcified with 0.25 M EDTA, pH 8.0, for at least 24 hr. Paraffin sectioning followed by H&E staining or IHC was performed at the Dana-Farber/Harvard Cancer Center Research Pathology Core. Primary antibodies included phospho-p44/42 MAPK (ERK1/2) (Thr202/Tyr204, Cell Signaling #4370; 1:150), phospho-AKT (Ser473, Cell Signaling #4060), phospho-S6 ribosomal protein (Ser240/244, Cell Signaling #4838), PCNA (PC10, EMD Millipore; 1:100), cleaved caspase-3 (Cell Signaling #9664; 1:100), GFP (Abcam #6556, 1:150), LC3A/B (Cell Signaling #12741; 1:200), HSP90 (Cell Signaling #4874; 1:100), and HSP70 (Enzo #ADI-SPA-810; 1:25). Antibody binding was detected with either a diaminobenzidine-peroxidase (DAB) visualization system (EnVision+, Dako, Carpinteria, CA) or a Bond Polymer Refine Red Detection Kit (Leica Biosystems, Buffalo Grove, IL). Mayer's hematoxylin was used for counterstaining.

Imaging and quantification

For brightfield DIC images, a Zeiss Axio Imager.Z1 compound microscope equipped with an AxioCam HRc was used. For live imaging, zebrafish were anaesthetized using 0.016% tricaine (Sigma) and mounted in 3% methylcellulose (Sigma). A Nikon SMZ1500 microscope equipped with a Nikon digital sight DS-U1 camera was used for capturing both the brightfield and fluorescent images from live zebrafish. For melanoma quantification, all animals in the same experiments were imaged under the same conditions, and the acquired fluorescent images were quantified using the ImageJ software by measuring the pigment or EGFP fluorescence. The pigment or fluorescent area was normalized against the surface area of the fish head to control for varying size of fish. Overlays were created using ImageJ and Adobe Photoshop 7.0.1.

Drug treatment

After 2 days of post-transplantation recovery, the 3-week-old juvenile *rag2*$^{-/-}$ fish transplanted with *nf1/pten*-mutant melanoma cells were randomly separated and treated with trametinib (Selleck Chemicals, Houston, TX), cobimetinib (Selleck), buparlisib (Selleck), apitolisib (Selleck), sirolimus (rapamycin, LC Laboratories, Woburn, MA), everolimus (LC Laboratories), temsirolimus (LC Laboratories), sorafenib (LC laboratories), sabutoclax (Selleck), obatoclax (Santa Cruz), chloroquine (Sigma), olaparib (Selleck), venetoclax (Chemietek, Indianapolis, IN) and S63845 (Chemgood, Glen Allen, VA) with refreshment every 2 days. Sample size was estimated according to https://www.statstodo.com/SSizSurvival_Pgm.php, that with at least 10 animal per group, we will have 90% power to identify 20% tumor suppression, or 95% power to identify 50% tumor suppression, testing at the 0.05 one sided level using a log-rank test. The drug treatment experiments were all blinded that the drug administration and tumor progression monitoring were performed by independent investigators. The treatment conditions were unblinded after the completion of tumor monitoring. Each experiment was replicated at least three times in the laboratory.

Western blots and antibodies

Whole-cell lysates were prepared in RIPA buffer. Protein concentration was quantified with a Pierce BCA Protein Assay Kit (Thermo Fisher Scientific Inc.). Equivalent amounts of protein were diluted in the Laemmli samples buffer (Bio-Rad Laboratories) and separated by SDS-PAGE. Proteins were transferred to PVDF membranes (Millipore, Billerica, MA) and subjected to immune blot analysis with each of the specific antibodies for NF1 (Bethyl Laboratories #A300-140A-M; 1:2000 dilution), PTEN (Cell Signaling #9188; 1:1000 dilution), total ERK1/2 (Cell Signaling #4695; 1:1000 dilution), and cleaved caspase 3 (Cell Signaling #9661; 1:500 dilution). All primary antibodies were diluted in 5% milk in PBST (0.5% Tween-20 in PBS).

He *et al*, Figure 1

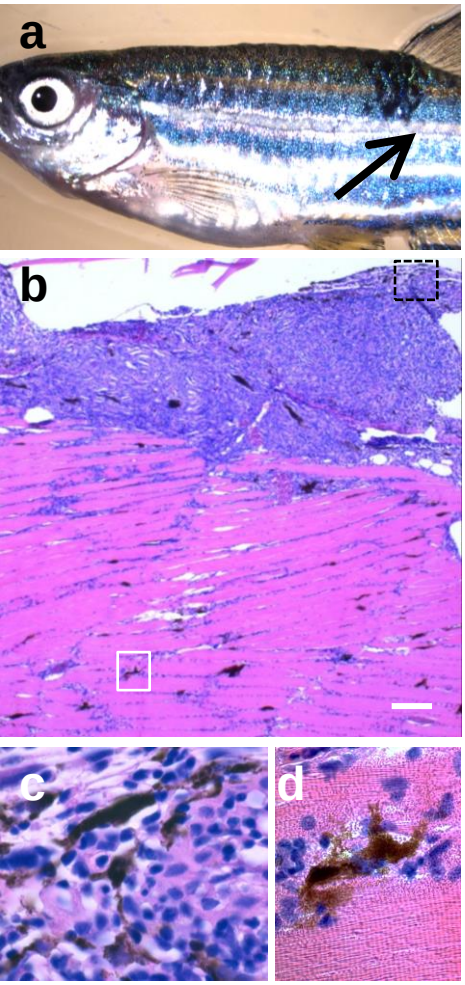

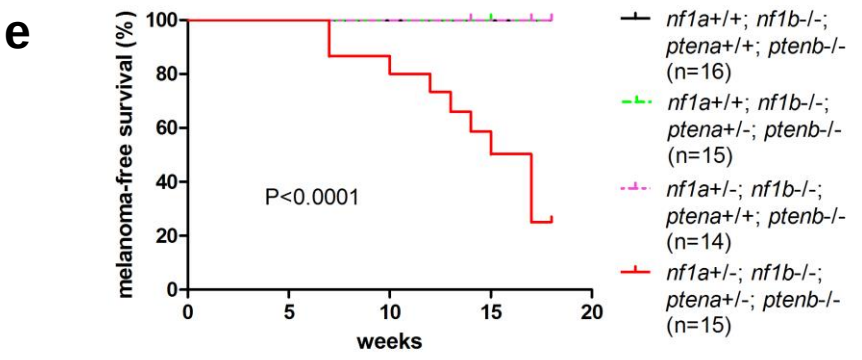

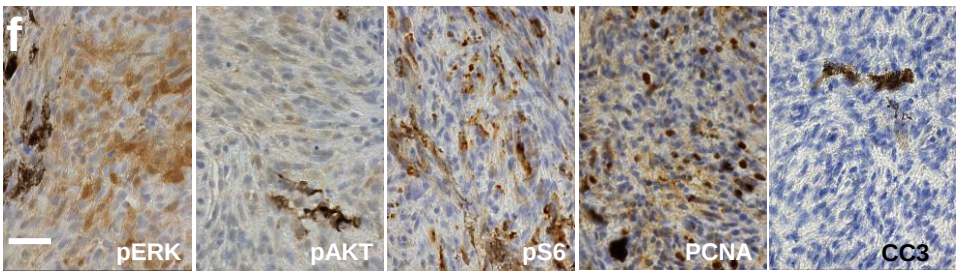

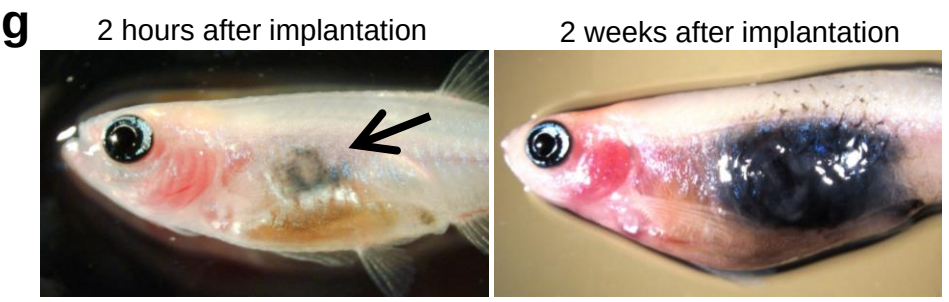

He *et al*, Figure 2

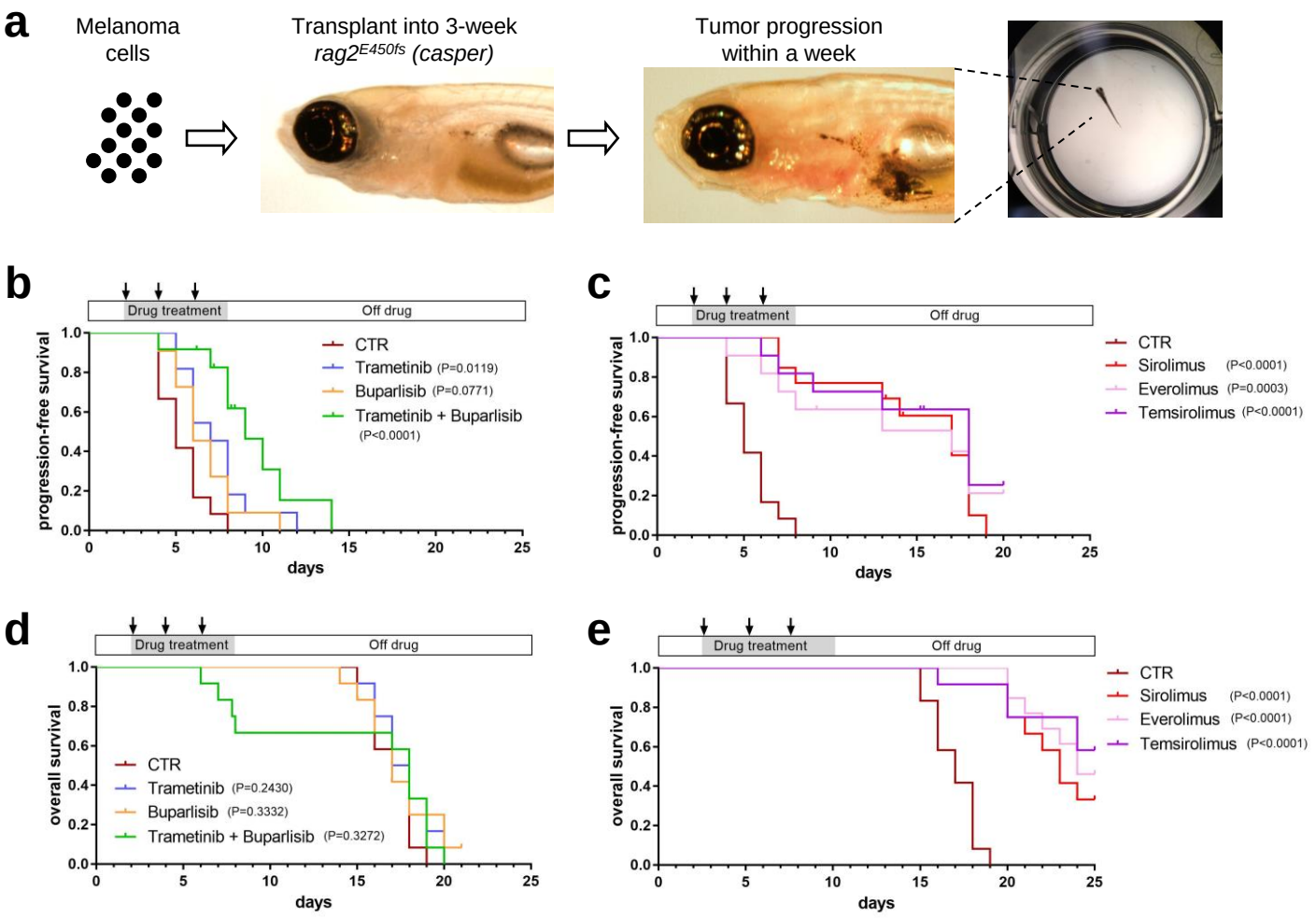

He *et al*, Figure 3

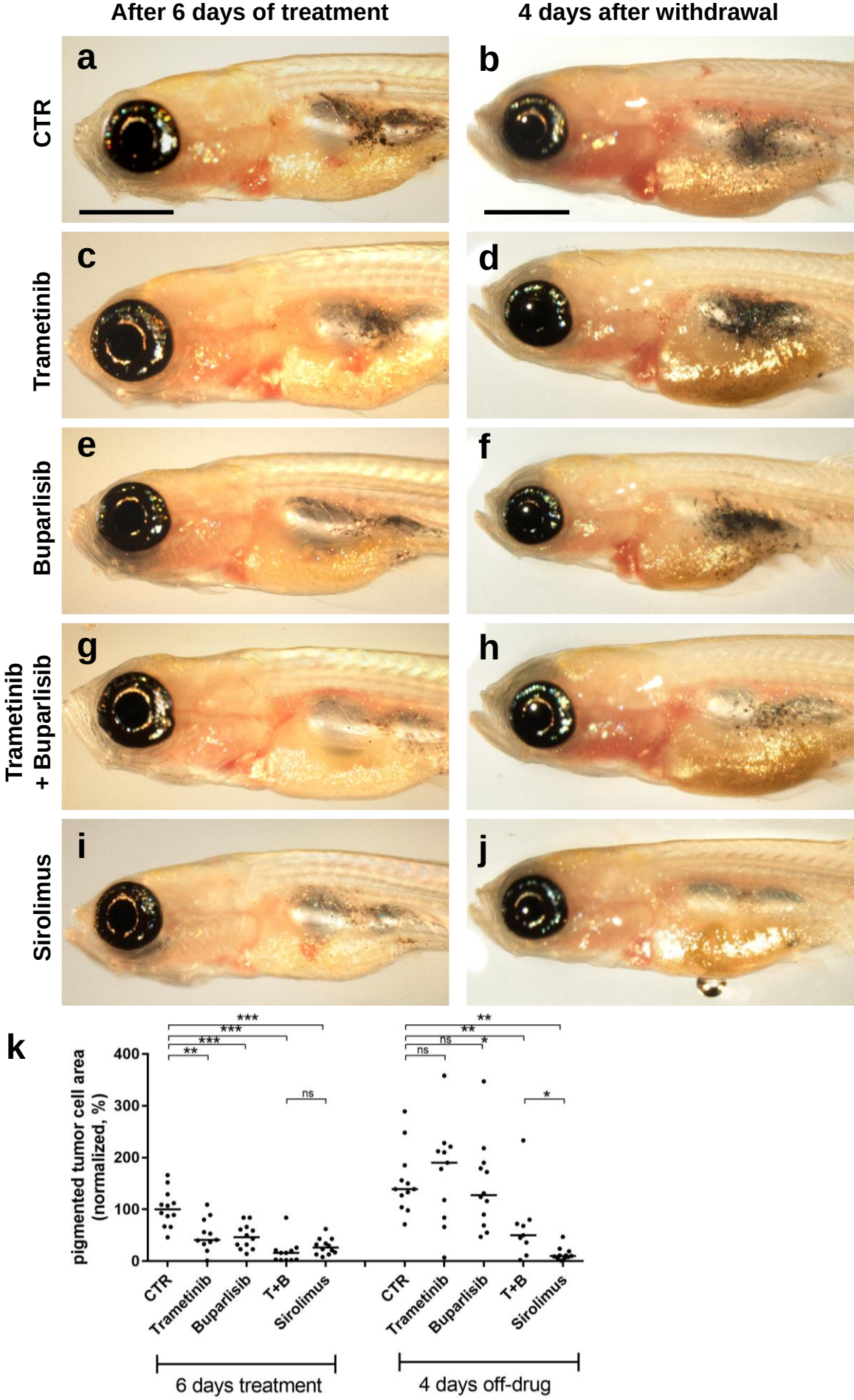

He *et al*, Figure 4

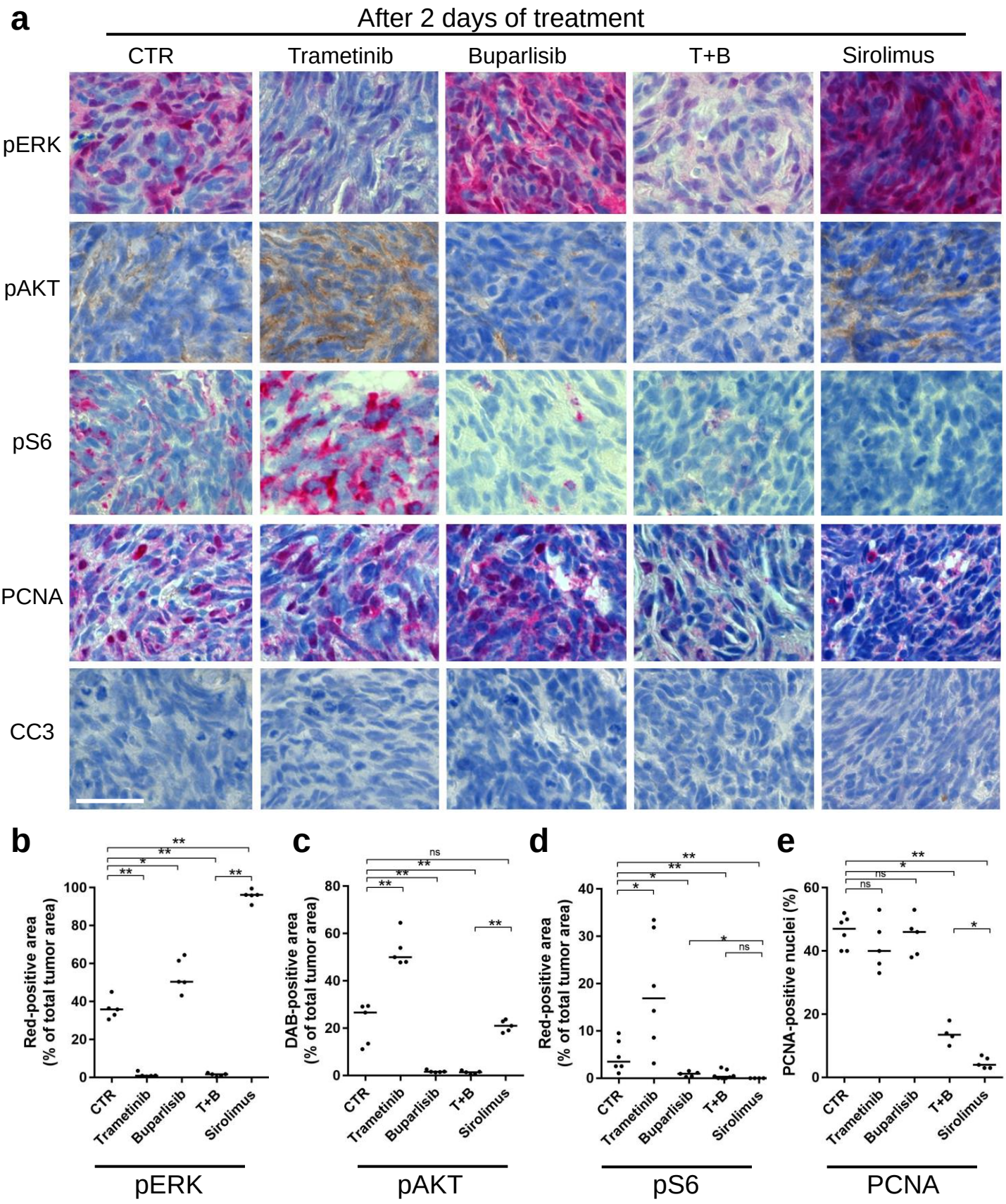

He *et al*, Figure 5

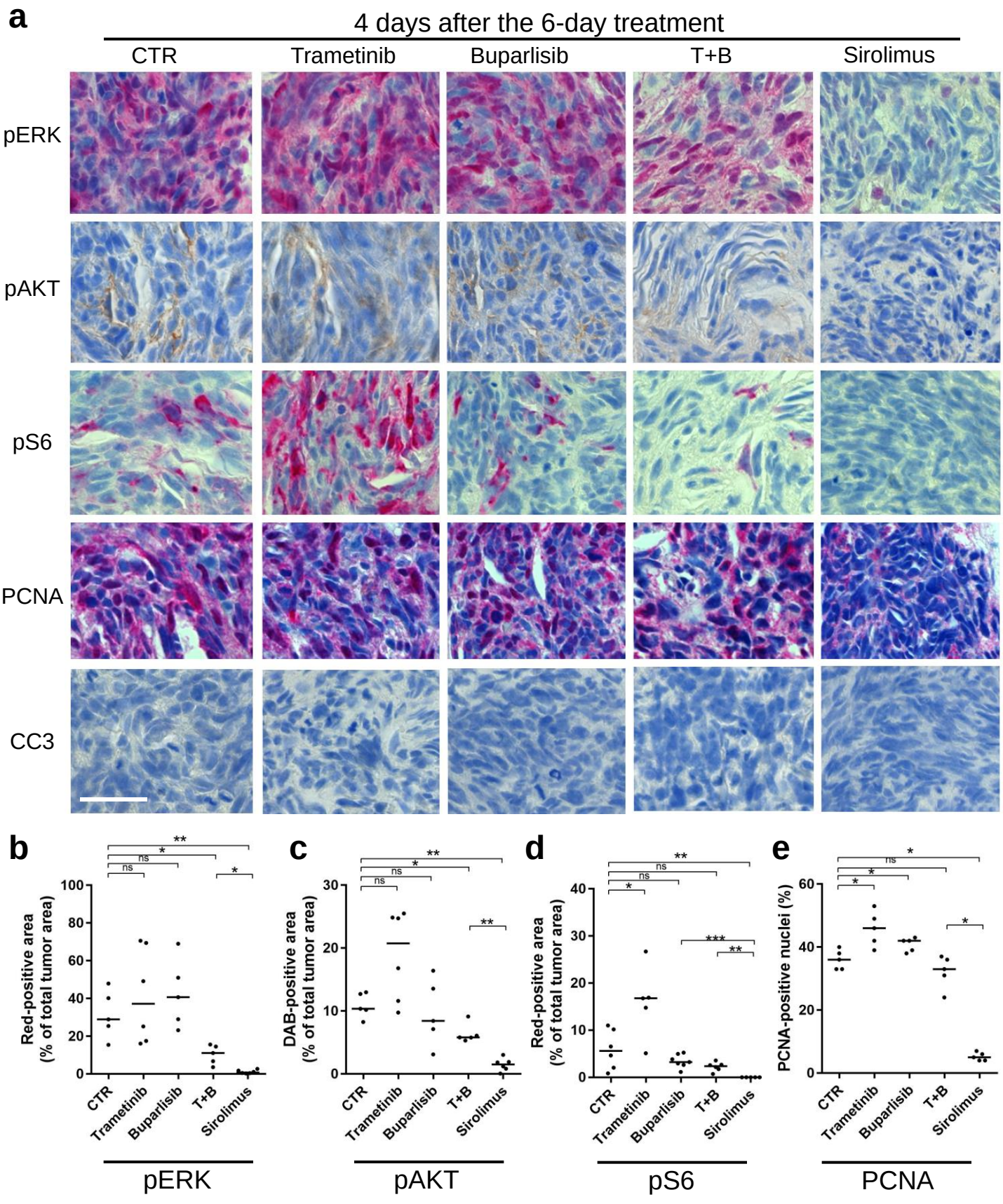

He *et al*, Figure 6

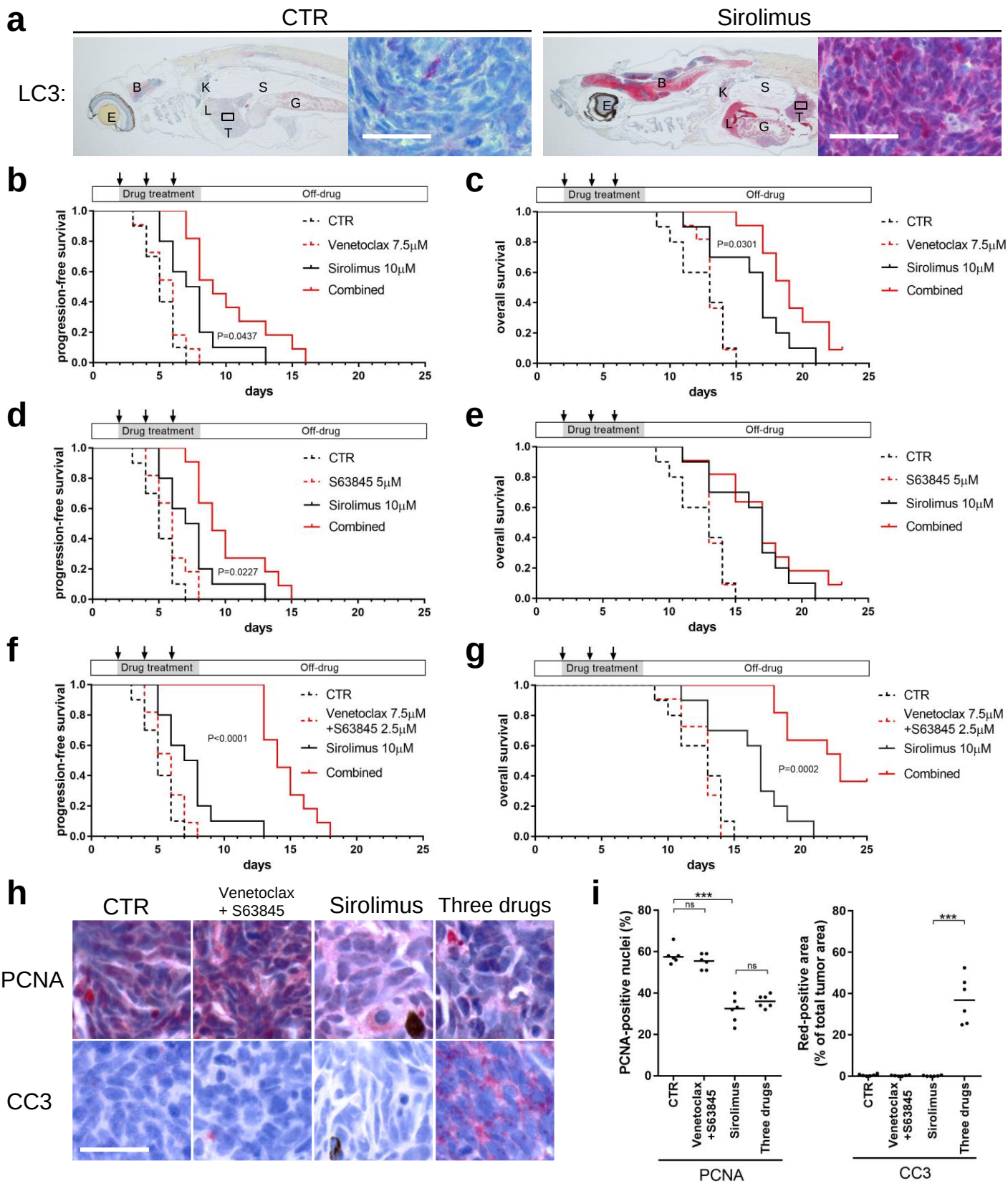

He *et al*, Figure 7

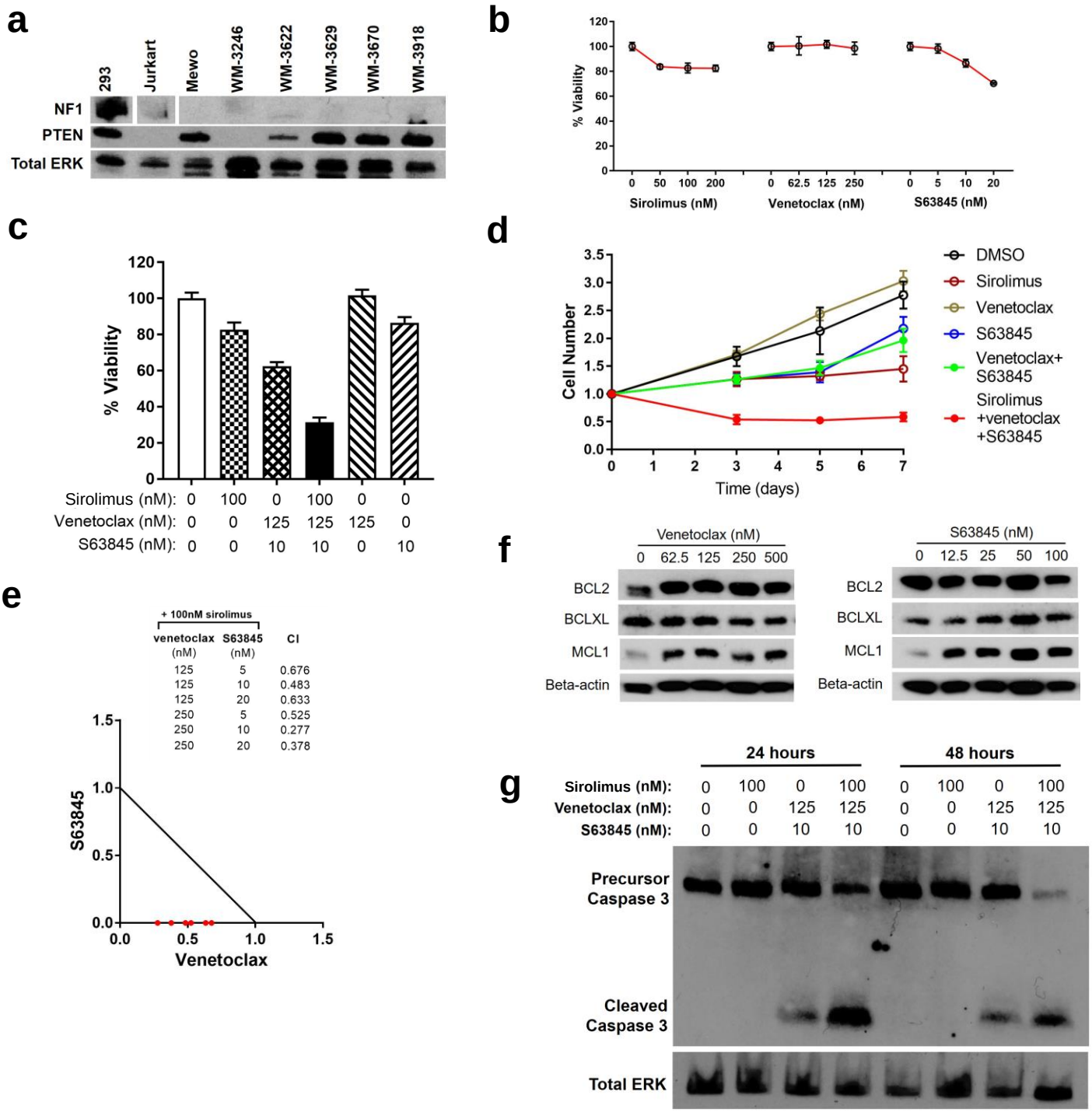

He *et al*, Supplementary Figure 1

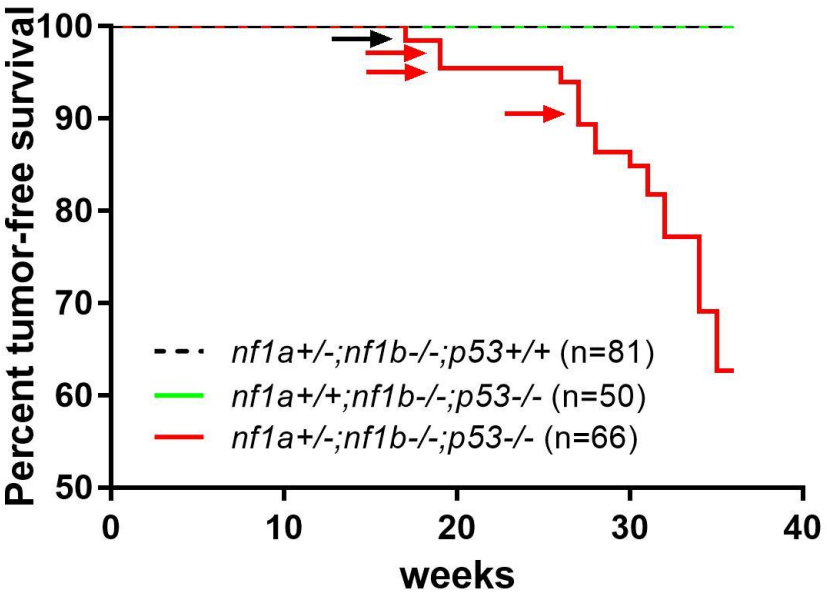

He *et al*, Supplementary Figure 2

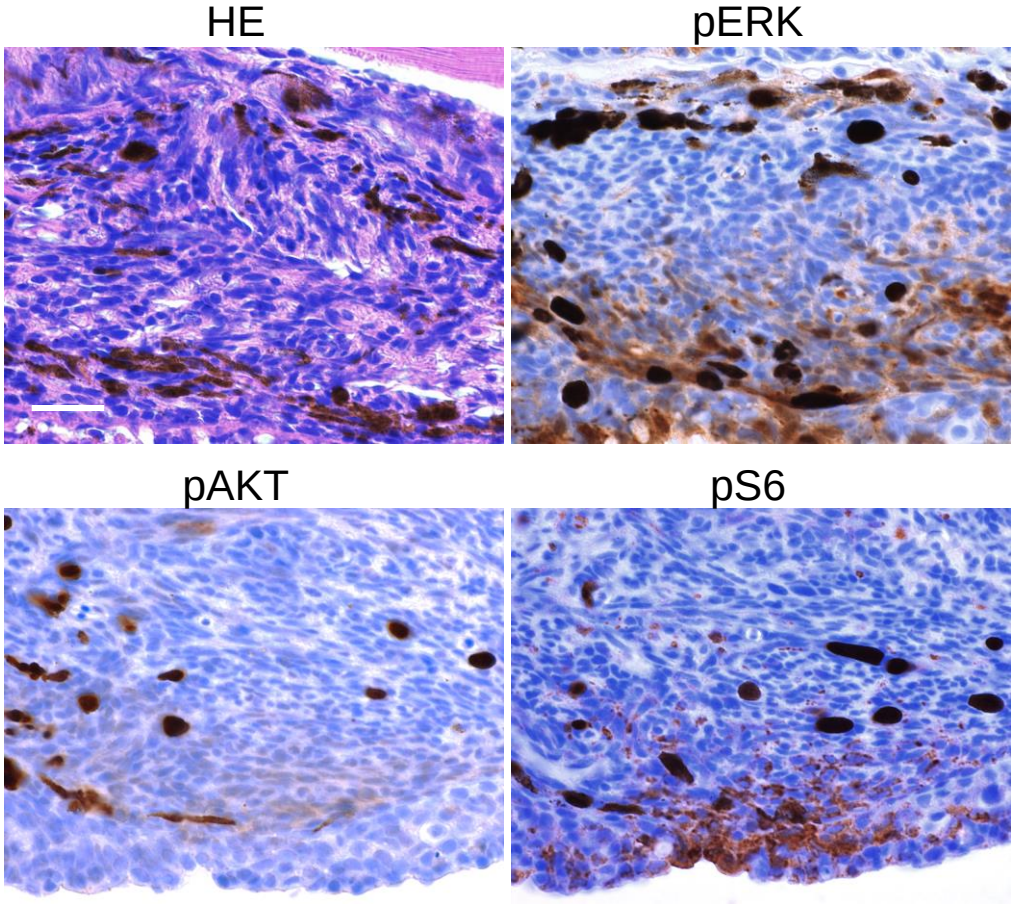

He *et al*, Supplementary Figure 3

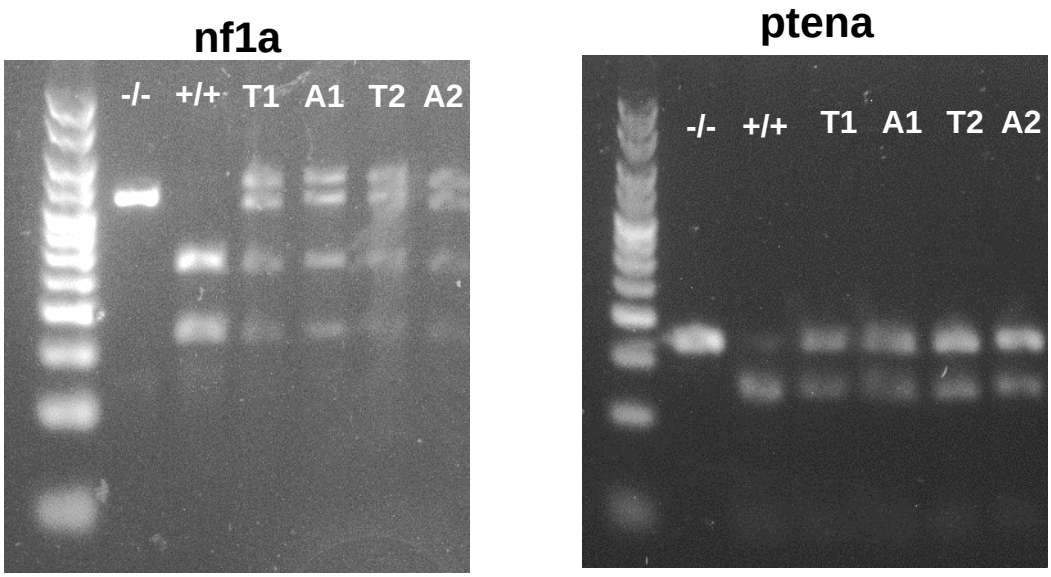

He *et al*, Supplementary Figure 4

a

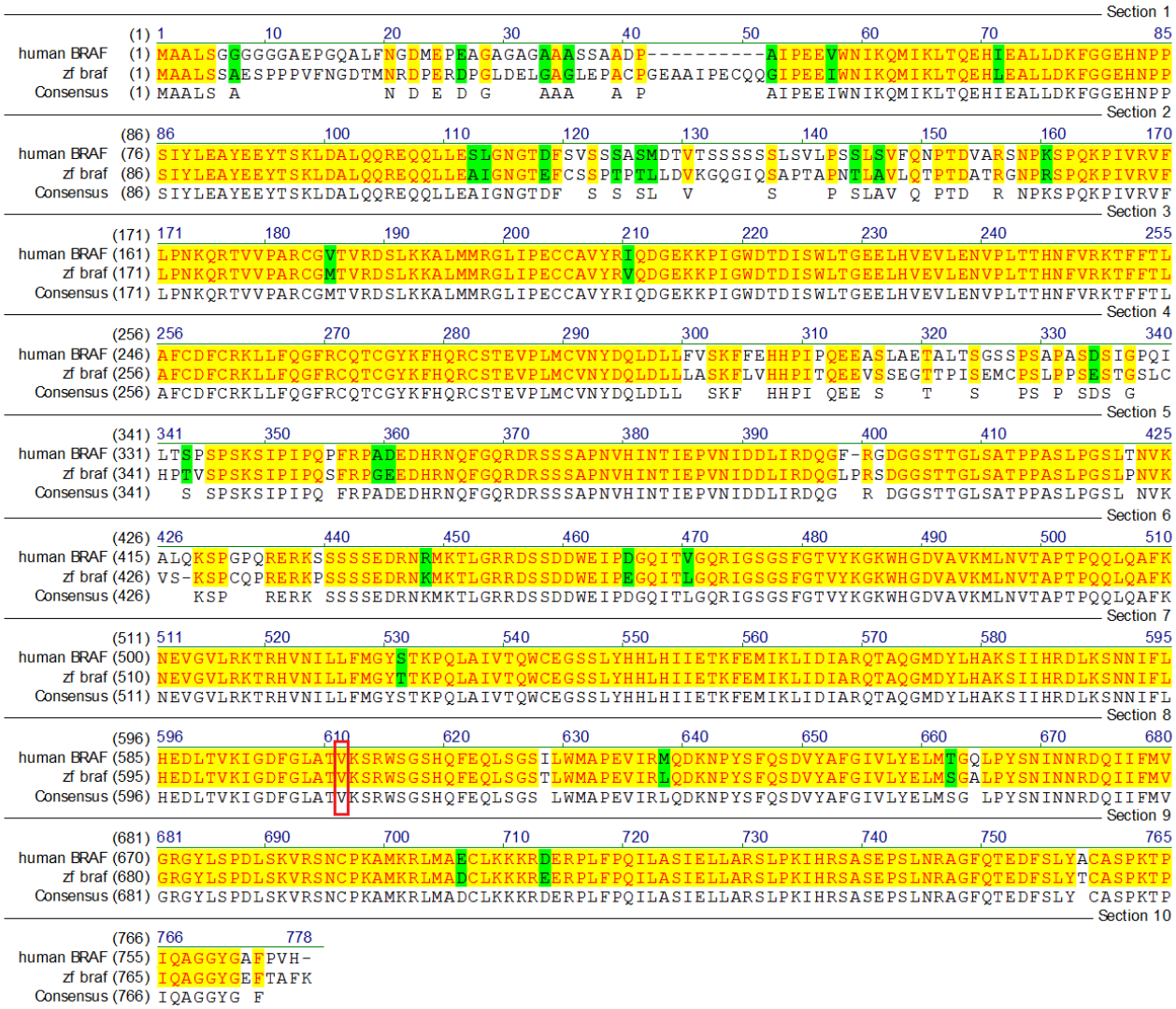

b

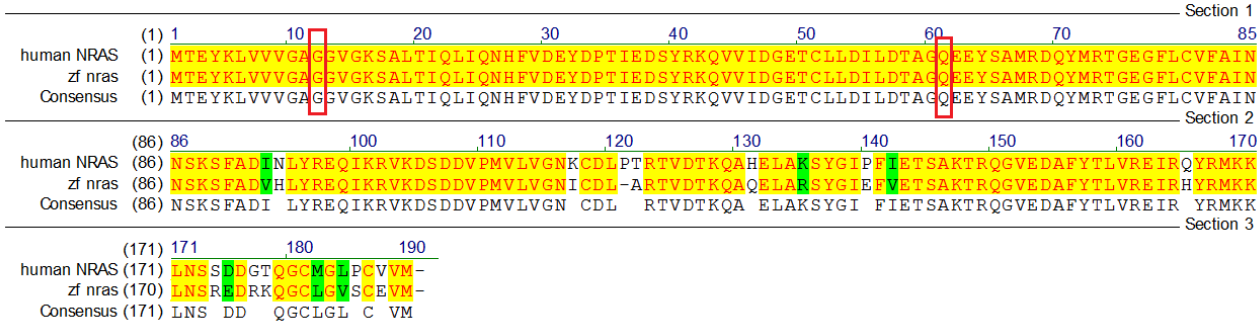

He *et al*, Supplementary Figure 5

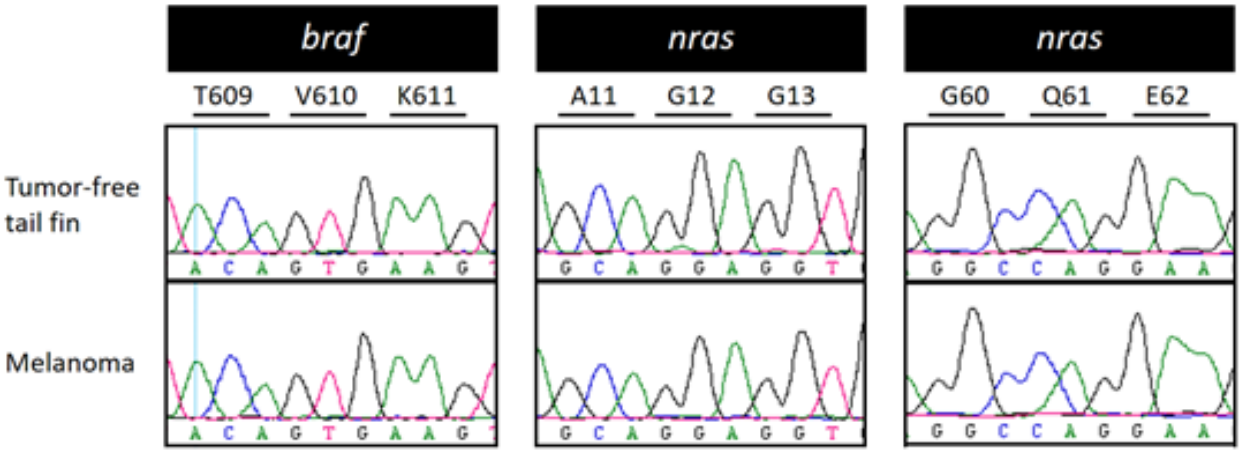

He *et al*, Supplementary Figure 6

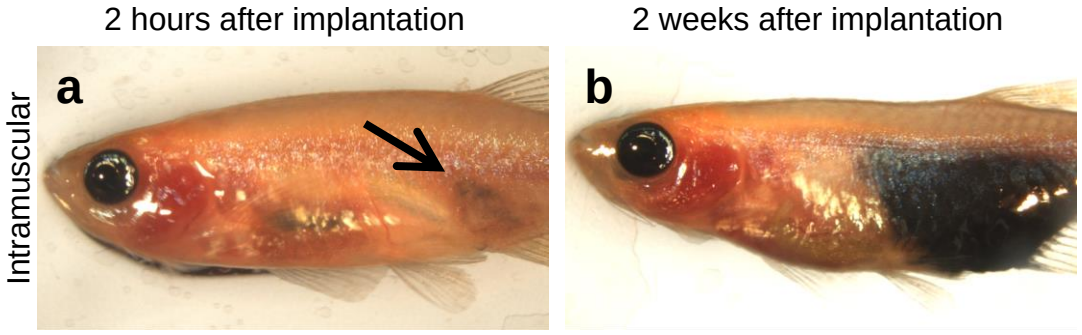

He *et al*, Supplementary Figure 7

a

Trametinib (nM) / Buparlisib (μM)

Buparlisib (μM) \ Trametinib (nM)	0	20	40	80	100
0	3	3	3	3	0
0.5	3	3	3	3	-
1	3	3	3	3	-
2	3	3	3	3	-
4	0	-	-	-	-

Cobimetinib (μM) / Apitolisib (μM)

Apitolisib (μM) \ Cobimetinib (μM)	0	0.2	0.5	1	2	5
0	3	3	3	3	2	0
1	3	3	1	0	0	-
2	3	2	0	0	0	-
5	3	0	0	0	0	-
10	0	-	-	-	-	-

b

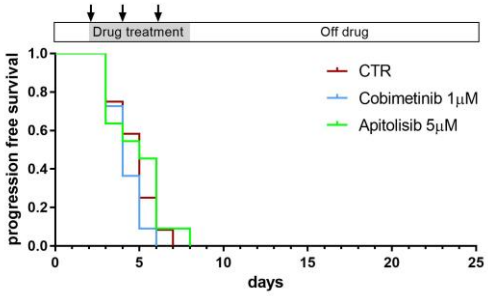

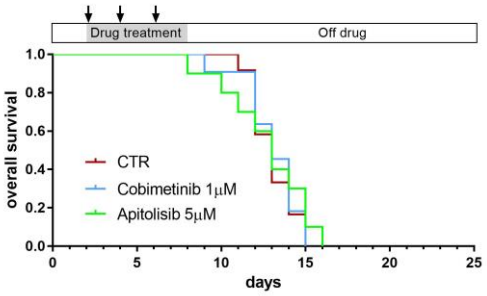

He *et al*, Supplementary Figure 8

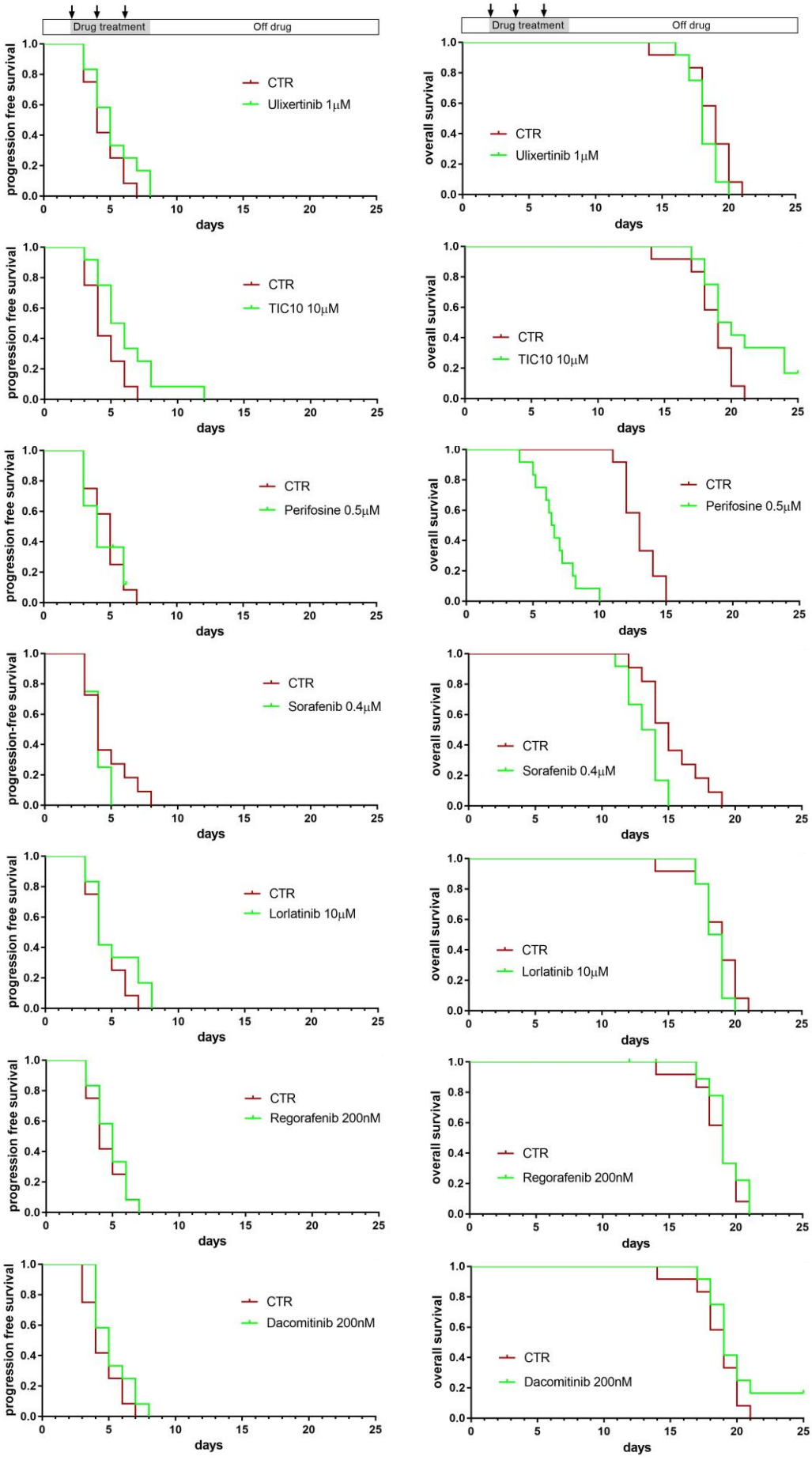

He *et al*, Supplementary Figure 9

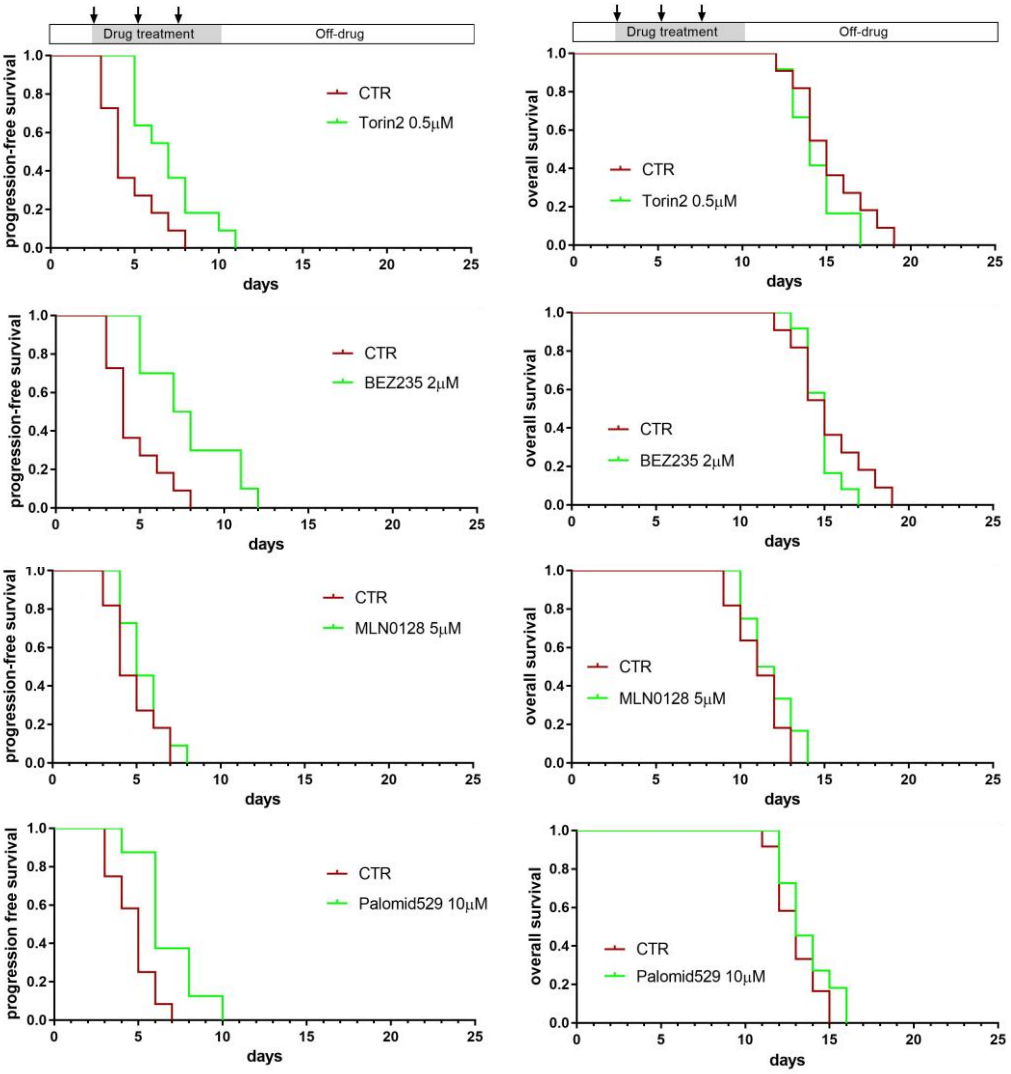

He *et al*, Supplementary Figure 10

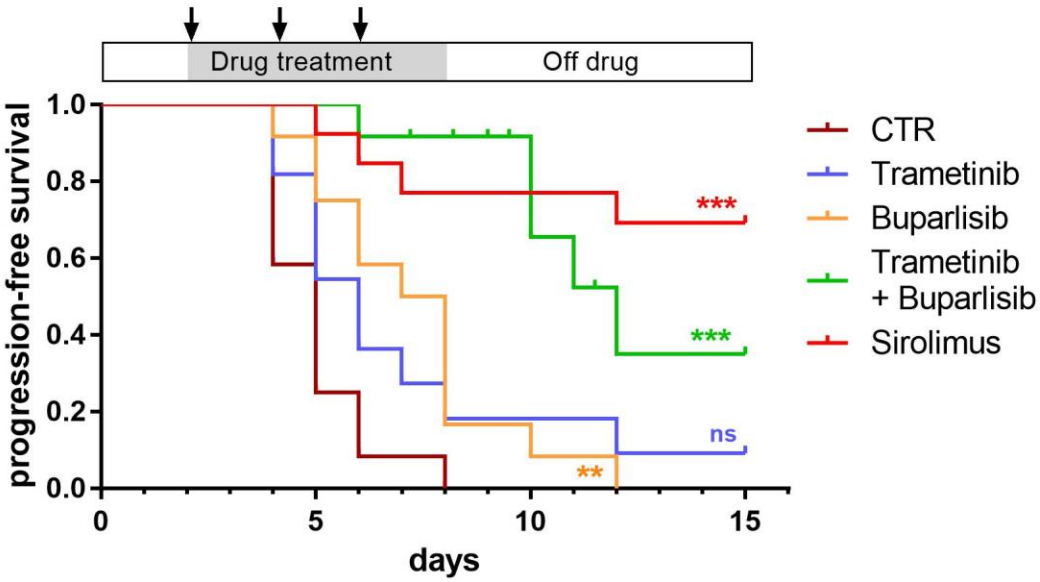

He *et al*, Supplementary Figure 11

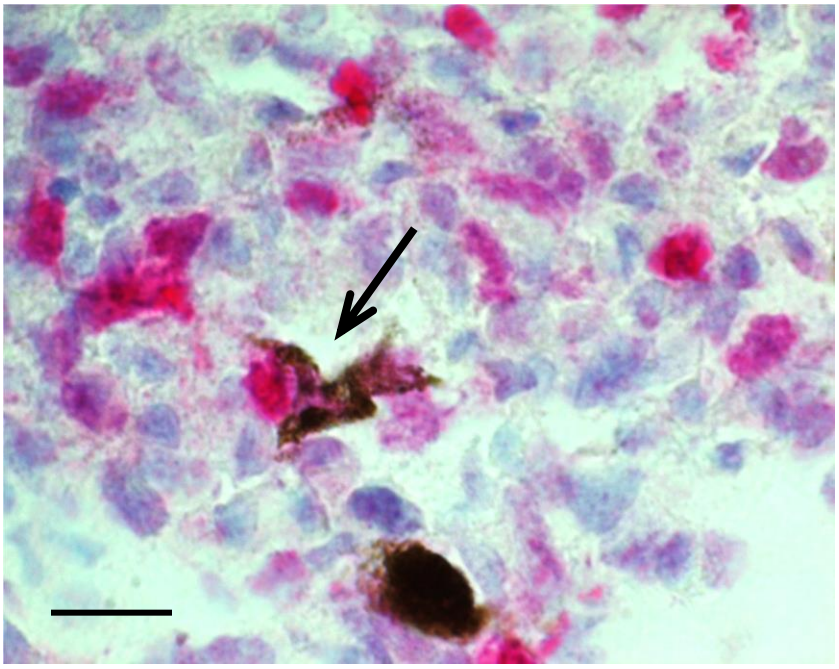

He *et al*, Supplementary Figure 12

a

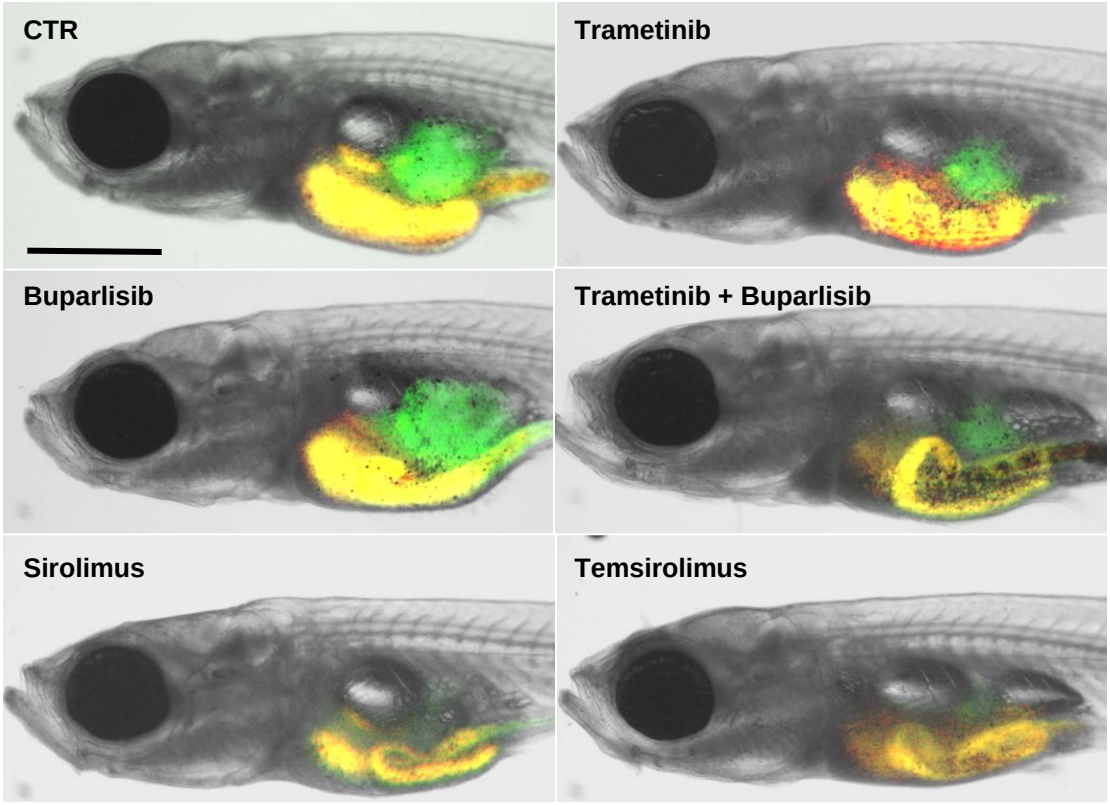

b

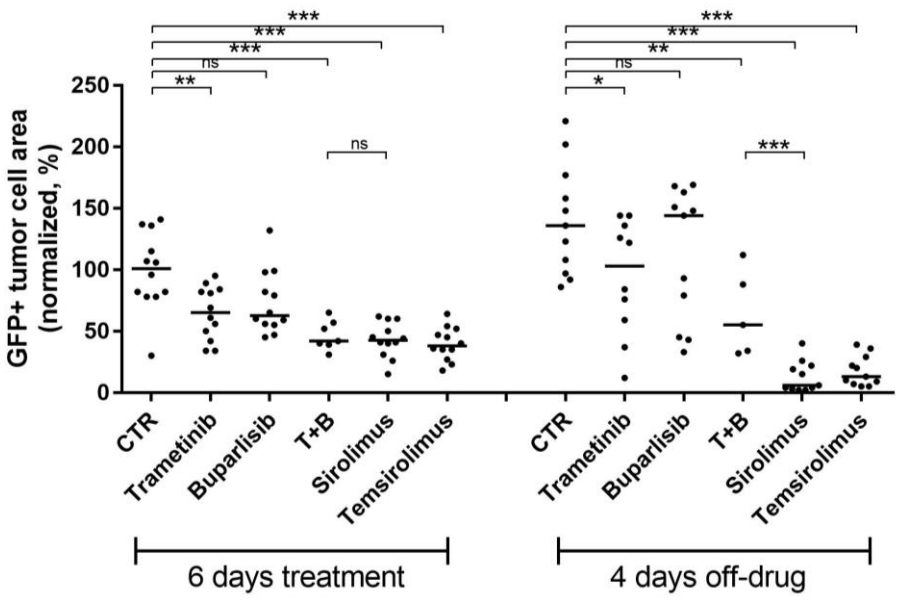

He *et al*, Supplementary Figure 13

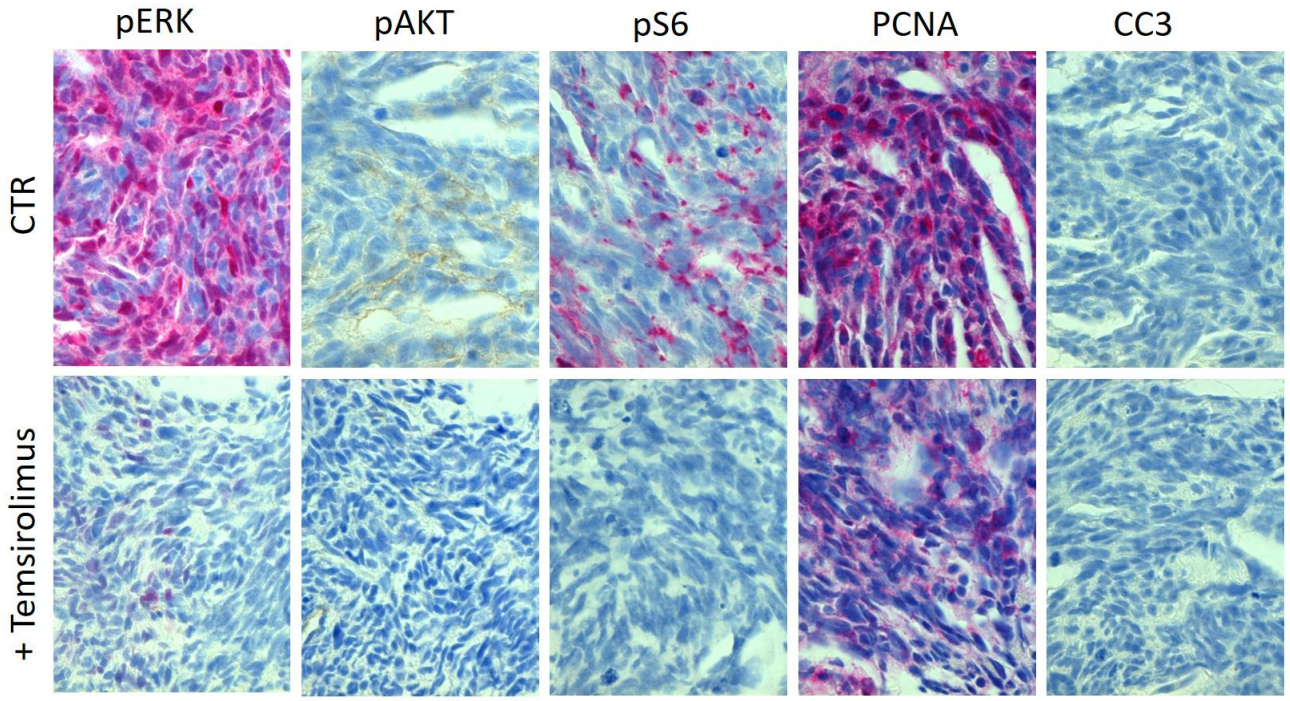

He *et al*, Supplementary Figure 14

Two drug combinations:

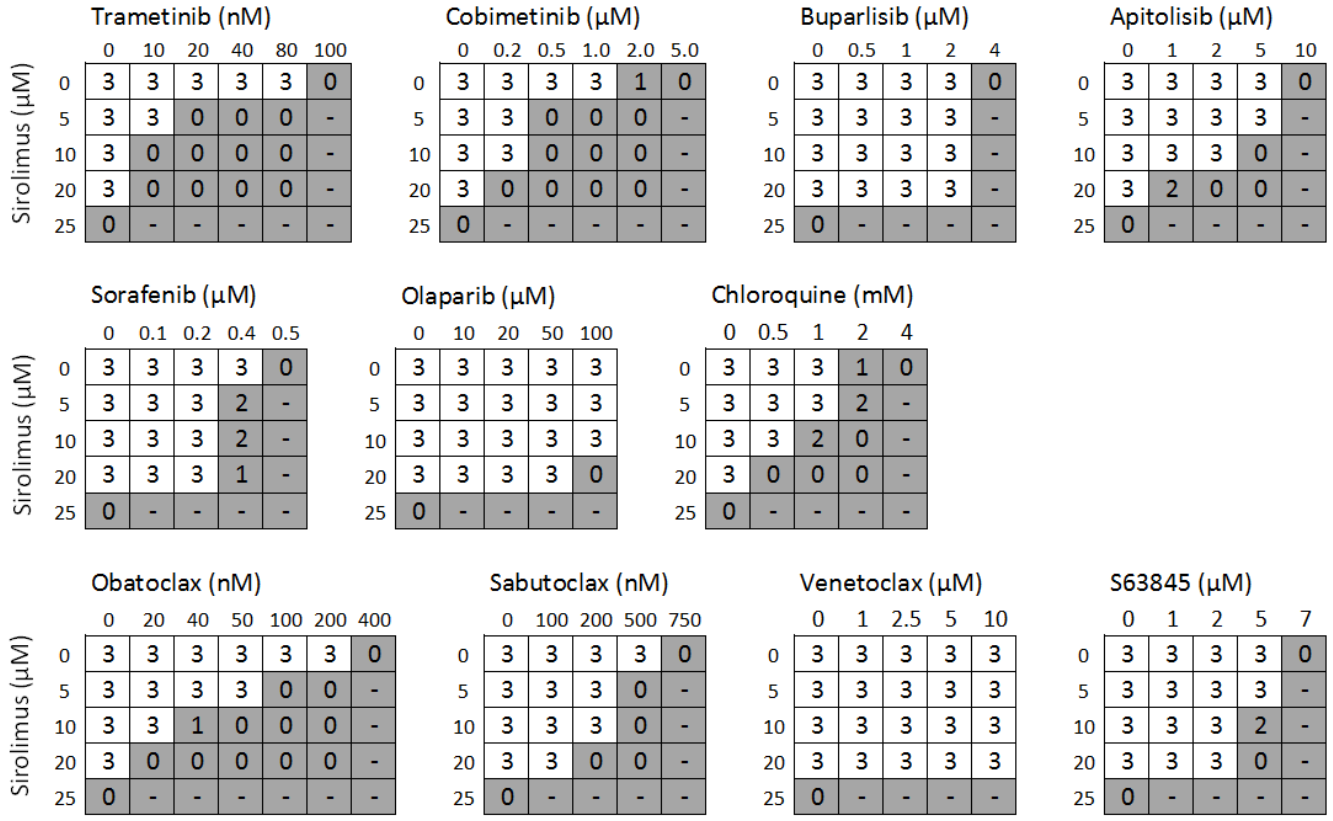

Three drug combination:

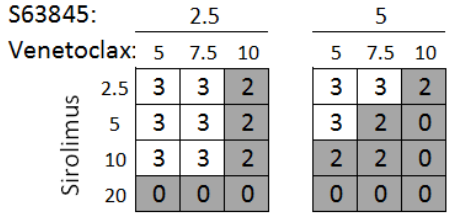

He *et al*, Supplementary Figure 15

Kinase inhibitors

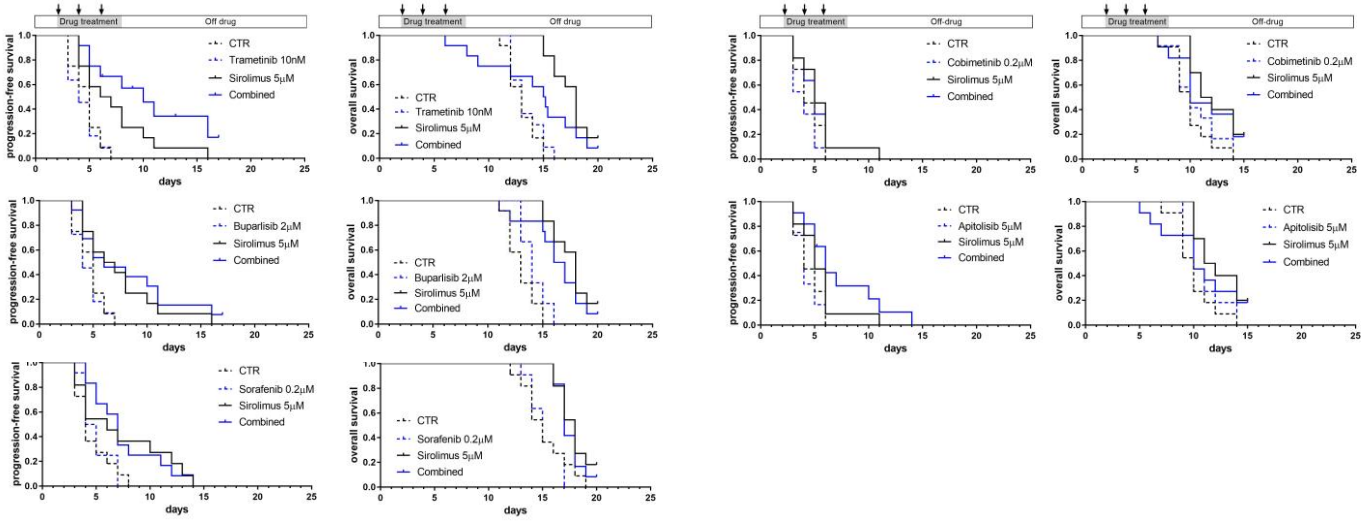

PARP1 inhibitor

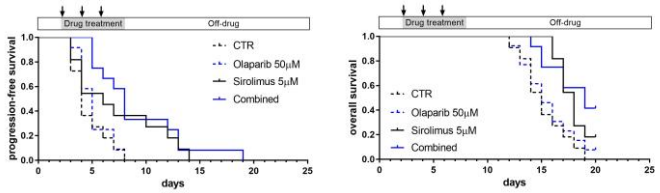

Autophagy inhibitor

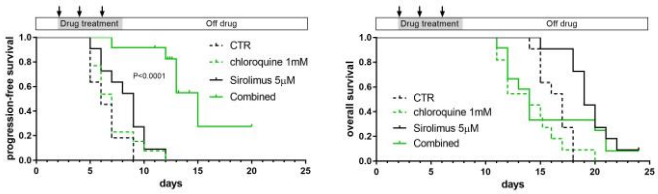

Inhibitors against BCL2-family of prosurvival proteins

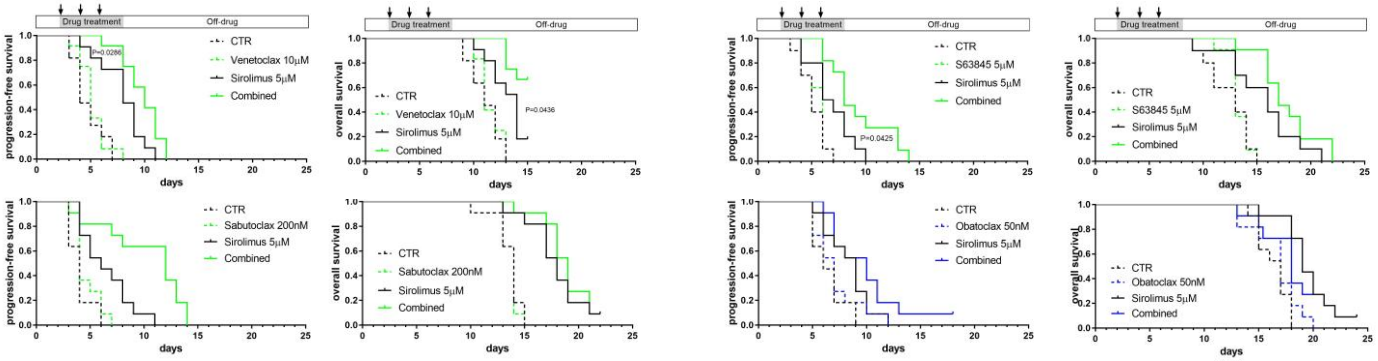

He *et al*, Supplementary Figure 16

a

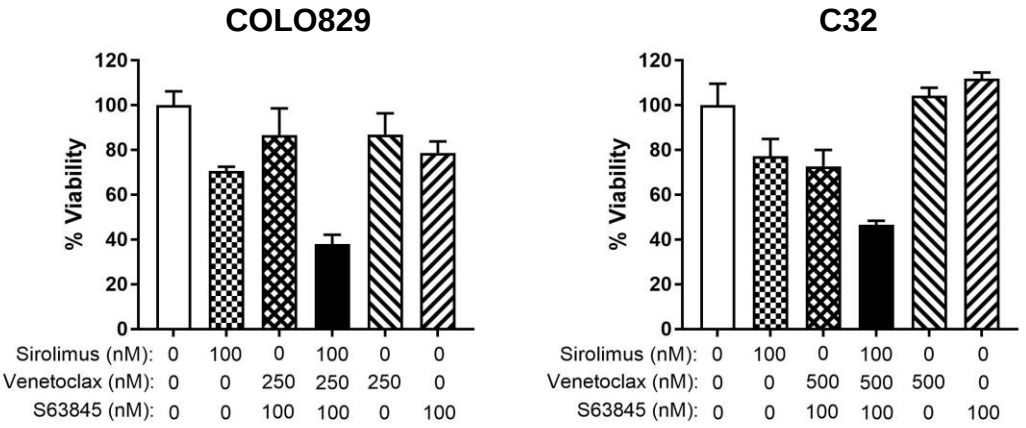

b